



FLEXURAL INTENSITY MEASUREMENT ON FINITE PLATES USING MODAL SPECTRUM IDEAL FILTERING

A. NEJADE AND R. SINGH

*Acoustics and Dynamics Laboratory, Department of Mechanical Engineering,
The Ohio State University, Columbus, OH, U.S.A. E-mail: armand_nejade@yahoo.com*

(Received 26 July 2000, and in final form 5 December 2001)

Flexural intensities on various plate-like structures with arbitrary boundary conditions are calculated using measured and FEM yielded mobility. In doing so, a two-dimensional spatial Fourier transform has been implemented along with a refined k -spectral filtering concept. Intensity is decomposed into individual contributions from bending moments, twisting moments and shear forces. The source and energy sink localization and energy flow have been analyzed through these contributions. The effect of reflections from the plate edges and that of the uncorrelated noise, on the intensity, are discussed. It is shown that the width of the k -filters may have a non-negligible influence on the shape of the intensity field. Damping in the structure can efficiently control the edge reflections and therefore help to localize the energy sources and sinks. A link has been found, at certain excitation conditions, between the radiated acoustic intensity and the active flexural intensity. It is also observed that the classical method of studying the vibration transmission, using vibration amplitude measurements, does not reflect the transmitted vibration energy but rather provides information on non-propagating, reactive energy. The FEM study, further explains some of the experimental observations and suggests the possibility of applying intensity to complex analytical models.

© 2002 Elsevier Science Ltd. All rights reserved.

1. INTRODUCTION

In this pioneering work of 1970 [1] Noiseux undertook some experiments on plates that produced original, but due to the lack of experimental sophistication, incomplete results. The development of the structural intensity formulations by Pavic [2] led to a growing interest in this field during the last two decades. However, the body of literature has mostly focused on beams. Plate intensity formulae with terms comprised of first, second and third order spatial derivatives pose quite an experimental challenge, especially when one has to solve them through finite difference techniques. Williams *et al.* [3] introduced the acoustic holography technique to estimate structural intensity in plates. By measuring the acoustic pressure on a plane parallel to the structural surface and by using the Green theorem, they calculated the plate's surface velocity. The structural intensity was then estimated using Pavic's formulae [2]. This approach enabled them to determine both structural and acoustic intensities through sound pressure measurements and consequently to study structural sound radiation problems. Another novel idea in this work consisted of the utilization of the spatial Fourier transform (SFT) and k -space low-pass filtering, rather than traditional finite difference techniques, to evaluate the spatial derivatives of the surface velocity. These techniques were then applied to a free-free rectangular plate to localize the excitation sources; but the structural modal behavior was not examined. The holography

technique needs to be extended to the study of bounded plates whose radiation behavior includes the acoustic cancellation effects [4] or acoustically inefficient frequencies. Although very attractive, holography measurements themselves may also add a new and significant error source to already sensitive intensity calculations.

Application of the (SFT) has been addressed further in articles by Zhang and Adin Mann [5, 6]. The authors carry out a parallel investigation of both Pavic's and Romano's [7] intensity formulations; the latter incorporating additional terms related to the shear deformation and rotary inertia effects. They show that at low frequencies, where such effects are negligible, both formulations produce the same results. Their experimental work considers the middle section of a large plate with large amount of damping and anechoic boundaries. The focus is on the source localization and the influence of a rib on the intensity field. Some issues regarding the utilization of k -space low-pass filtering and spatial windowing using band-pass k -filtering are briefly addressed. k -Space filtering is further treated by Spalding and Adin Mann [8]. In these latter works however, the effects of boundary conditions and plate modes on the intensity field are not examined. Morikawa and Ueha [9] have also approached the problem of plate intensity measurements through the SFT. As a result of a comparative study, they establish the superiority of SFT over the finite difference method. These authors also examine the effects of low-pass k -space filtering on the intensity measurements and the optimal cut-off wave number for such a filter. Through some experiments, they deduce an empirical relationship. Although good results are obtained for their example (the middle section of a free-free plate but heavily damped outside the measurement area), the behavior of such filters still remains to be further investigated.

Other researchers tackle the problem of intensity in plates by using analytical approaches. Gavric and Pavic [10] use the finite elements (FEM) results to directly evaluate the intensity as a scalar product of stress and the surface velocity. The FEM solutions provide the stresses in the middle of element while the velocities are obtained at element nodes. Through an interpolation, they project nodal velocities to the middle of elements and hence calculate intensity at these points. The examples shown consider only simply supported plates. This approach is dependent on the accuracy of the computational model, especially when non-ideal boundary conditions are present. Bouthier and Bernhard [11] consider the far field of an infinite system and develop an approximate solution to the flexural wave equation. None of the analytical approaches investigates the reactive intensity and its correlation with structural modal characteristics.

In this article, the SFT approach is adopted to estimate flexural intensity in finite plates with arbitrary boundary conditions. The k -space filtering is implemented in relation to the modal superposition principal. Flexural intensity examples are demonstrated for plates with non-ideal boundary conditions and free-free conditions and for an irregularly shaped free-free plate. The free-free plates are used for source and damping patch localization and deformation studies. Energy flow, energy transmission and sound radiation issues are investigated in the context of a gearbox top plate where the structural intensity and sound intensity are studied in parallel. Finally, an analytical computation using finite element modelling is carried out to further investigate the effects of uncorrelated noise, edge reflections and damping on the intensity. A detailed analysis of the reactive part of intensity aims for a clearer understanding of this entity.

2. FLEXURAL INTENSITY FORMULATION

In thin plate theory, i.e., with $\lambda_b \gg h$ over the frequency range of interest, the effects of shear deformation and the rotary inertia effects are ignored. The overall time-averaged

intensity expressions in x and y directions are given by [2]

$$I_x(x, y) = D \left\langle \left[\frac{\partial}{\partial x} (\nabla^2 w) \frac{\partial w}{\partial t} - \left(\frac{\partial^2 w}{\partial x^2} + \nu \frac{\partial^2 w}{\partial y^2} \right) \frac{\partial^2 w}{\partial x \partial t} - (1 - \nu) \frac{\partial^2 w}{\partial x \partial y} \frac{\partial^2 w}{\partial y \partial t} \right] \right\rangle_t, \quad (1a)$$

$$I_y(x, y) = D \left\langle \left[\frac{\partial}{\partial y} (\nabla^2 w) \frac{\partial w}{\partial t} - \left(\frac{\partial^2 w}{\partial y^2} + \nu \frac{\partial^2 w}{\partial x^2} \right) \frac{\partial^2 w}{\partial y \partial t} - (1 - \nu) \frac{\partial^2 w}{\partial x \partial y} \frac{\partial^2 w}{\partial x \partial t} \right] \right\rangle_t. \quad (1b)$$

For practical purposes, it is more convenient to evaluate time-averaged harmonically varying intensities in the frequency domain. With $\tilde{W}(x, y, \omega) = F \{w(x, y, t)\}$, the intensity formulae adopt the following forms:

$$\tilde{I}_x(x, y, \omega) = \text{Im} \{ \tilde{I}_x \} - j \text{Re} \{ \tilde{I}_x \}, \quad \tilde{I}_y(x, y, \omega) = \text{Im} \{ \tilde{I}_y \} - j \text{Re} \{ \tilde{I}_y \}, \quad (2a, b)$$

where \tilde{I} 's are defined as

$$\begin{aligned} \tilde{I}_x(x, y, \omega) &= \frac{D}{2\omega} \left[\frac{\partial}{\partial x} (\nabla^2 \tilde{W}) \tilde{W}^* - \left(\frac{\partial^2 \tilde{W}}{\partial x^2} + \nu \frac{\partial^2 \tilde{W}}{\partial y^2} \right) \frac{\partial \tilde{W}^*}{\partial x} - (1 - \nu) \frac{\partial^2 \tilde{W}}{\partial x \partial y} \frac{\partial \tilde{W}^*}{\partial y} \right], \\ \tilde{I}_y(x, y, \omega) &= \frac{D}{2\omega} \left[\frac{\partial}{\partial y} (\nabla^2 \tilde{W}) \tilde{W}^* - \left(\frac{\partial^2 \tilde{W}}{\partial y^2} + \nu \frac{\partial^2 \tilde{W}}{\partial x^2} \right) \frac{\partial \tilde{W}^*}{\partial y} - (1 - \nu) \frac{\partial^2 \tilde{W}}{\partial x \partial y} \frac{\partial \tilde{W}^*}{\partial x} \right]. \end{aligned} \quad (3a, b)$$

The three terms in the brackets are associated with the shear force, the bending moment and the twisting moment energy contributions respectively [2, 12]. The real part of \tilde{I}_x and \tilde{I}_y is associated with the reactive part of the intensity.

In the following sections, different components of the flexural intensity, i.e., contributions from bending moments, shear forces and twisting moments will be represented individually. For the sake of brevity we will call them bending moment, shear force and twisting moment sub-intensities.

3. EVALUATION OF SPATIAL GRADIENTS

Intensity formulae (1) and (3) contain partial derivatives of up to the third order. To evaluate these derivatives from discretized data, where the measurements (or analogous analytical computations) are carried out at discrete spatial points, the approach proposed by Williams *et al.* [3], rather than the finite difference method, was used. This approach employs the spatial Fourier transform for the calculation of the partial derivatives. This is done by using the well-known formula

$$\frac{\partial^{m+n} w}{\partial x^m \partial y^n} = F^{-1} \{ (jk_x)^m (jk_y)^n F \{w(x, y)\} \}. \quad (4)$$

Here, F and F^{-1} are the direct and inverse 2-D spatial Fourier transforms, defined as

$$\begin{aligned} W(k_x, k_y; \omega) &= F \{w(x, y; \omega)\} = \frac{1}{4\pi^2} \int_{-\infty}^{\infty} \int_{-\infty}^{\infty} w(x, y; \omega) e^{-j(k_x x + k_y y)} dx dy, \\ w(x, y; \omega) &= \int_{-\infty}^{\infty} \int_{-\infty}^{\infty} W(k_x, k_y; \omega) e^{-j(k_x x + k_y y)} dk_x dk_y. \end{aligned} \quad (5a, b)$$

Numerical algorithms used to calculate the spatial Fourier transforms from discretized samples (spatial DFT, in this case), including MATLAB [13] in this work, produce double-sided spectra. It is therefore necessary that, as equation (4) implies, each component of the Fourier transform be multiplied by the related value of k as determined by [14]

$$k_n = \frac{2\pi}{L}(n-1), \quad \text{at } n \leq N/2; \quad k_n = 0 \quad \text{at } n = \frac{N}{2} + 1,$$

$$k_n = \frac{2\pi}{L}(n-N-1) \quad \text{at } n > \frac{N}{2} + 1 \quad \text{where } n = 1, 2, \dots, N. \quad (6)$$

4. METHOD IMPLEMENTATION AND ERROR SOURCES

Since the intensity estimates in plate structures represent products of very small quantities, they are very susceptible to measurement errors. Among many sources of error, phase instability and noisy spectral components appear to be very important.

4.1. PHASE INSTABILITIES AND CHOICE OF EXCITATION

Because the intensity formulae (equations (3)) deal with complex velocities, the intensity is very sensitive to the phase relationship among signals. Phase instabilities in cross power spectrum estimations must be minimized to reduce intensity distortions. A proper choice of the excitation signal is therefore important especially for a structure of large dimensions and/or with low damping. This is because here, the reverberation time is long and when excited by fast varying signals (such as random noise or chirp) the structure cannot reach its steady state.

Although a pure tone tends to be the most stable choice, its application is obviously quite time consuming even when a "multi-sine" is used (a synthesized signal, given by $\xi(t) = A \sum_i \sin \omega_i t$, with arbitrarily selected frequencies ω_i). An alternative to the usage of a pure tone signal is the swept sine excitation $A \sin \omega(t)t$, with a slow sweep rate S , as suggested by the ISO standard [15] on mobility measurements:

$$S_{max} < 54 (f_r)^2 (\eta_r)^2 \quad \text{Hz/min.} \quad (7)$$

The swept sine excitation produced results as stable as those of pure sine excitation.

4.2. MODAL SUPERPOSITION AND SPECTRAL FILTERING

When a system is excited through a single frequency ω , all of its eigenmodes are excited but with various degrees of strength, as expressed by the well-known modal superposition equation:

$$\{\tilde{W}\} = \sum_{r=1}^N \frac{\{\phi\}_r^T \{F\} \{\phi\}_r}{(\omega_r^2 - \omega^2) + j\eta_r \omega_r^2}. \quad (8)$$

The overall shape of the structure is therefore a specific combination of all its natural mode shapes. The importance of the contribution of each mode to the overall shape depends on the proximity of the corresponding eigenfrequency to the frequency of the excitation.

The wave number spectra resulting from equation (5a) include contributions from the various modes of the structure. In experimental situations, the uncorrelated noise may have a significant presence in the spectrum. This is particularly effective at wave numbers at or near low energy modes and could cause significant errors. The leakage caused by spatial data truncation may also affect the k -spectrum. A combination of these phenomenon can be observed in Figure 1(a), where a double-sided 2-D Fourier transform of velocities, measured on a free-free steel plate, is illustrated. The plate was excited by a pure tone at 1432 Hz. The strong k -components, seen at each corner, correspond to the structural wave number defined by

$$k_s = \frac{\sqrt{\omega}}{\sqrt[4]{D/\rho_s}} \quad (9)$$

and its adjacent modes. The other components represent the weak modes and uncorrelated noise. Using a wide wave number spectrum in the calculation of intensity will therefore lead to the presence of strong noise components observed in Figure 1(a). These may interact with the intensity vectors, resulting in an “smeared” view of the field, as it will be further discussed in section 6.2.7. To diminish such effects, the intensity field must incorporate a limited number of k -components. To remove the unwanted components in k -spectra, we apply a uniform spectral window to the discrete Fourier transform. One example of such procedure is illustrated in Figure 1. Figure 1(a) represents a 2-D k -spectrum of a real plate having strong noise components. Figure 1(b) illustrates the same spectrum where only two k -components at each side of the structural wave number k_s of the plate have been retained.

When, in a plate, the frequency of excitation equals the eigenfrequency of the mode (m, n), then the structural wave number k_s , calculated from equation (9), will match the corresponding wave number $r_{m,n} = \sqrt{r_m^2 + r_n^2}$. In most cases, the excitation wave numbers do not match any of the eigenmodes and therefore k_s 's lie between two modal wave numbers r_p and r_{p+1} (here $p = 1, 2, 3 \dots$). In both cases however, the intensity information is conveyed by the modal wave numbers $r_{p-q}, r_{p-q+1}, \dots, r_p, r_{p+1}, \dots, r_{p+q}$, where $q = 0, 1, 2, \dots$. These becomes less and less significant as q increases, implying that most of the desired information is still concentrated in the few pairs of spectral wave numbers (k 's)

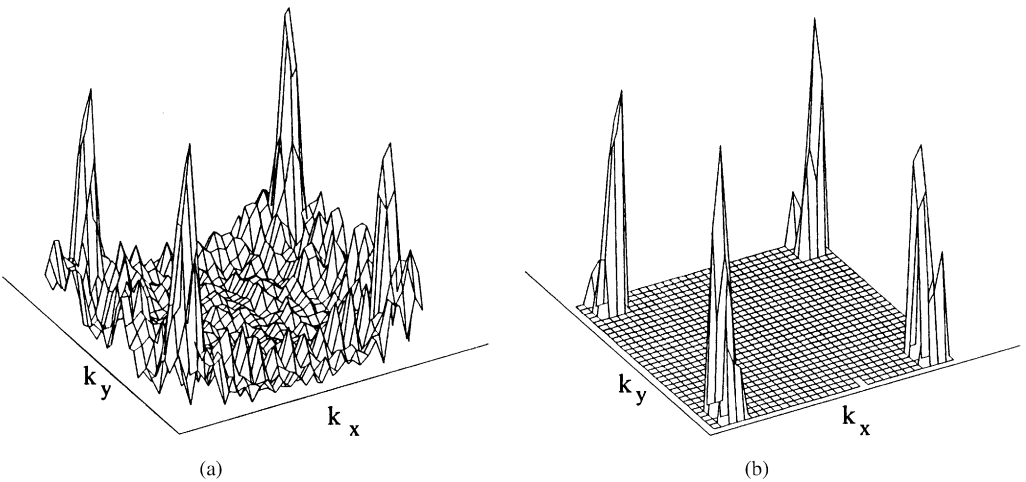


Figure 1. Measured double-side Fourier transform amplitude of a free-free plate when excited at 1432 Hz. (a) “Raw” Fourier transform versus k_x and k_y ; (b) transform with spectral filtering. Filter covers two pairs of k -components adjacent to k_s .

neighboring r_p and r_{p+1} . (Here, a distinction should be made between modal wave numbers r_i and spectral wave numbers k_j . The latter represents the sampled wave number components in discrete Fourier transform.) This fact is readily demonstrated by the high amplitude components in Figure 1.

All the wave numbers associated with the excited modes of the structure do contain, although in various degrees, information about the intensity field. But, they may also include noise. The compromise here was to resort to k -filtering (ideal filtering of k -spectrum) operations. The width $2q$ of these filters depends on the selected number of k -components in the calculations. There may not, however, be a clear-cut rule as to the number of such modes within the band.

4.3. SPECTRAL FILTERING PROCEDURE

In determining the position and the width of k -filters, the k -domain resolution must be considered. In the Fourier transformation of spatial data, the orthogonal components of the spectral wave number $k_{m,n}$ of the mode $r_{m,n}$, are given by the axial terms $\alpha\pi m/L_x$ and $\beta\pi n/L_y$, and

$$k_{m,n} = \pi \sqrt{(\alpha m/L_x)^2 + (\beta n/L_y)^2}, \quad (10)$$

where $m, n = 1, 2, 3, \dots$ ($m, n = 0, 1, 2, \dots$ for free boundaries). Relation (10) allows, by a simple reiterative procedure, to identify the indices m and n of the closest mode to the excitation k_s . The spectral filter is centered at k_s and will include spectral wave numbers (k -components) adjacent to k_s . The number of pairs of k -components circumscribing k_s determines the width of the uniform filter. All the k -components outside the defined bandwidth will be set to zero. Coefficients α and β are determined by the spectrum k -resolution and associated with the zero-padding operation as discussed below.

In space sampling, as in time sampling, one often needs a higher resolution to enable one to represent particular cases, e.g., where the L equals an odd multiple of $0.5\lambda_b$ or where intermodal k -components are to be taken into consideration. To satisfy such requirements, we have applied the well-known technique in discrete time signal processing, i.e., zero padding. The coefficients α and β in equation (10) are associated with the zero-padding operation in the x and y directions respectively. With the original record length they should be equal to 2, in which case the k -components closely correspond to multiples of λ_b . When, however, the record length is doubled in any direction, through zero padding, the corresponding coefficient becomes equal to 1. This leads to the k -components closely associated with $0.5\lambda_b$. These coefficients proportionally decrease when the record length in the related direction is increased.

The spectral filtering approach appears to be preferable to the low-pass filtering concept [3, 5, 9] since such filters may include unwanted components at low waves numbers. Also, depending on the choice of filter cut-off frequency, too many or insufficient components above k_s may be included. A procedure similar to the proposed spectral filtering has been suggested earlier by Spalding *et al.* [8]. Our approach however relies on the structural property (k_s), rather than statistical calculations, to locate the useful wave number band.

5. EXPERIMENTS

In the following experiments, we explore the possibility of solving such problems as locating sources and energy sinks, vibration energy transmission and acoustic radiation.

They also aim for a detailed analysis of reactive intensity. Depending on the nature of the investigation, several types of structure were used. In all the data acquisitions, the time signals were weighted by a Hanning window and 64 spectral averages were made. The swept-sine and multi-sine were selected as the excitation signals. Since in the case of swept-sine, the sweeping time was longer than the record length, a time record overlap of 25% was implemented to avoid any loss of data. From the 256 transfer functions (accelerances) associated with each set of vibration measurement, one 16×16 matrix was extracted per excitation frequency. Each element of the matrix is the cross-mobility (accelerance divided by $j\omega$), associated with one measurement point on the plate.

5.1. SOURCE AND DAMPING CHARACTERIZATION

These studies were implemented on an $890 \times 890 \text{ mm}^2$, free-free steel plate of 2.5 mm thickness (Figure 2(a-c)) and on an irregularly shaped free-free steel plate of the same thickness (Figure 2(d)). The measurements were made on a $270 \times 340 \text{ mm}^2$ rectangular area in the middle of each plate. It is important to note that the measurement area dimensions are used as L_x and L_y , respectively, in equation (10). The argument behind this technique is that even a small section of the plate contains the signatures related to all the excited modes. In this work, zero padding has been used to double the record length and therefore enhance the resolution by a factor of two.

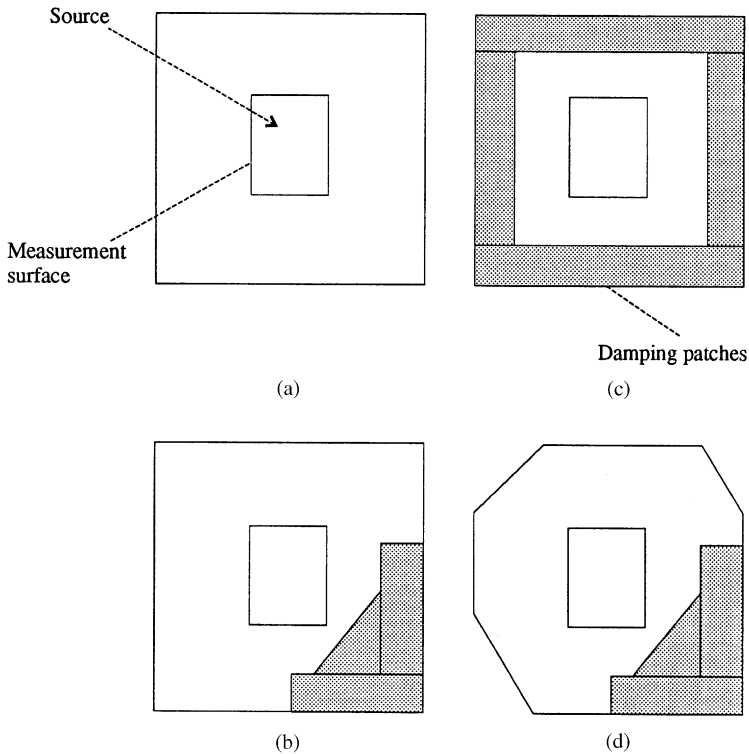


Figure 2. Free-free plate configurations used for active intensity analyses: (a) undamped plate, (b) plate with constraint layer damping concentrated at one corner on both faces, (c) plate with constraint layer damping along all the edges and on both faces, (d) an irregularly shaped plate with the same configuration of damping as in (b).

The plates were excited by a shaker normal to the surface at the co-ordinates (80, 240 mm) with respect to the lower left corner of the measurement areas illustrated in Figure 2. A force transducer was mounted between the plate and the shaker to provide the reference signal. Two type of excitation were tested. One was a swept sine covering the frequency range of 100–1600 Hz in 1.2 s and the other, a multi-sine signal comprising of 10 pure sines at selected frequencies, corresponding to some of the resonances as well as off-resonances of the plate. Both types of excitation produced similar results at common frequencies. Surface velocity measurements were carried out on 16×16 grid using six phase matched (within $\pm 0.1^\circ$) 1.5 g accelerometers. Such light mass accelerometers were used to avoid the effects of mass loading at the frequency range of interest. A multi channel FFT analyzer was used for the sequential data acquisitions and calculation of the transfer functions between the accelerations and the input force (Figure 3). Four experimental configurations were considered as shown by Figure 2: (a) the undamped plate; (b) a plate with constrained layer damping concentrated at one corner on both faces; (c) a plate with constrained layer damping along all the edges and on both faces; (d) an irregularly shaped plate with the same configuration of damping as in (b).

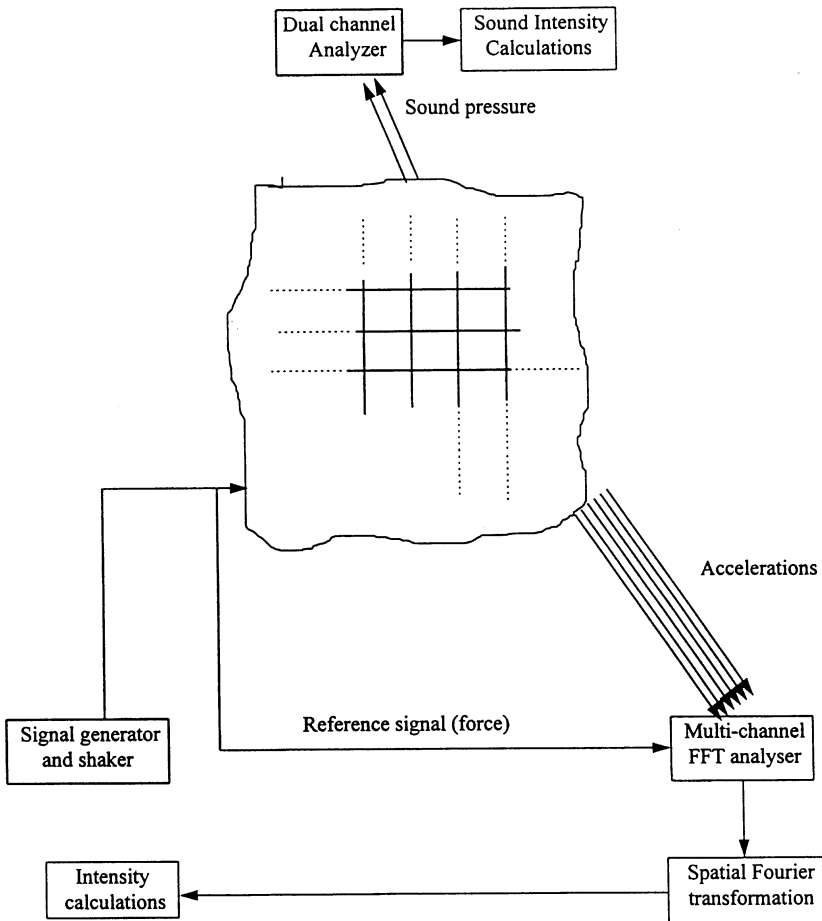


Figure 3. Experimental and instrumentation schematic including the measurement grid representation.

5.2. REACTIVITY INTENSITY

The reactive flexural intensity fields are investigated on the top plate of a gearbox described in section 5.3 as well as a free-free plate ($267 \times 343 \times 2.4 \text{ mm}^3$). The latter is excited, perpendicular to its plane, at a point of co-ordinates 80, 240 mm with respect to its lower left corner.

5.3. STRUCTURE BORNE SOUND RADIATION AND ENERGY TRANSMISSION

A model of a rotorcraft gearbox was used to investigate the energy transmission from, as well as the mechanism of generation of structure borne sound radiated by its top plate. The plate's dimensions are $L_x = 270 \text{ mm}$, $L_y = 340 \text{ mm}$ and $h = 6.35 \text{ mm}$. It is coupled to the four lateral plates of the box by screws, providing almost rigid boundary conditions. The whole gearbox is excited through its L-shaped shaft as illustrated in Figure 4. A force transducer mounted between the shaker and the L-shaped shaft produced the reference signal for the transfer functions (accelerances). Also, to estimate the structural intensity, the same vibration measurement procedures and equipment as in sections 5.1 and 5.2 were adapted to this structure. Acoustic intensity measurements however, were implemented using an 8×8 grid. These measurements were carried out, in all three Cartesian directions, on a surface parallel to and at 65 mm from the gearbox top plate (Figure 3). The intensity probe microphones spacing was 50 mm for measurements at the frequencies below 1000 Hz and 12 mm for the measurements at higher frequencies.

6. MEASURED RESULTS AND DISCUSSION

As a prelude to the analysis and to demonstrate the accuracy of spectral filters, let us consider the effects of the k -filter width on a plate's deformations. Here we reconstruct the

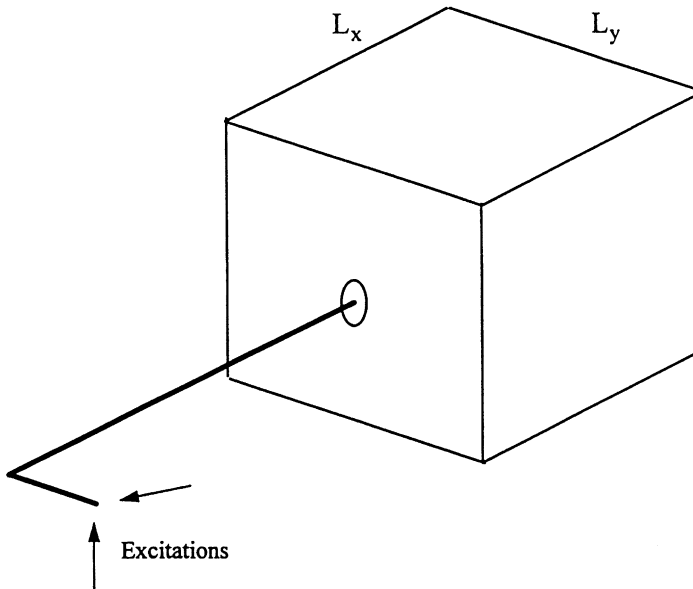


Figure 4. The gearbox whose top plate has been studied. L-shaped shaft is excited by shaker.

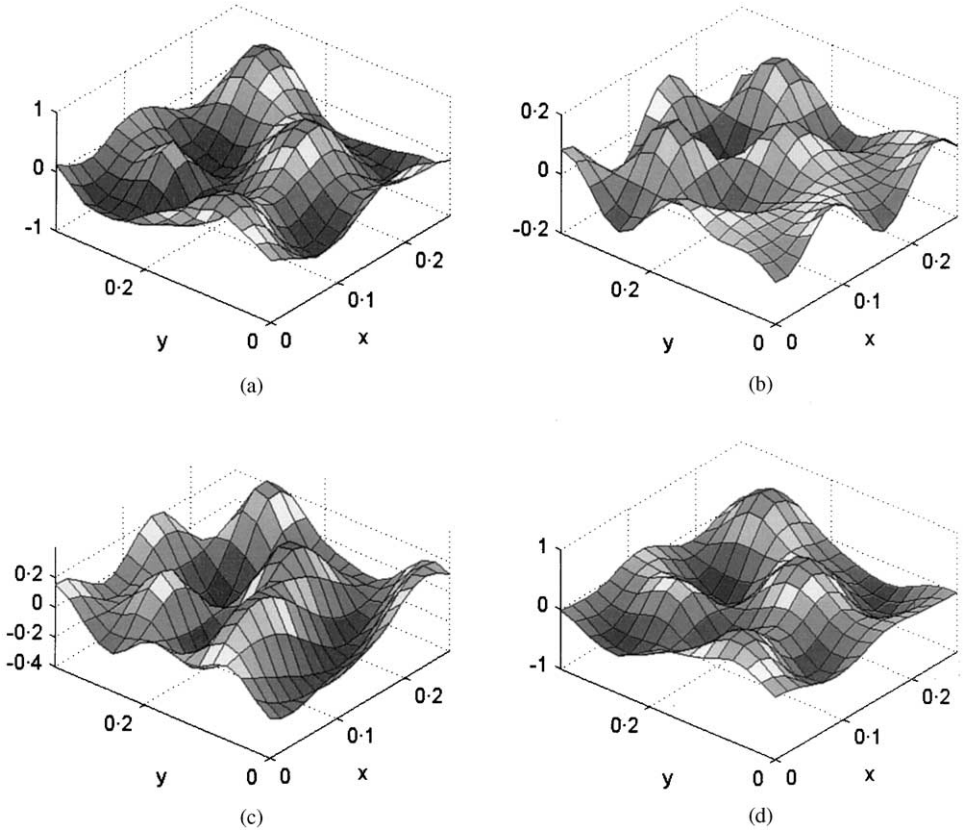


Figure 5. Effects of k -filter width on plate deformations. (a) Measured deformation of the measurement area in the middle of a free-free plate at 1058 Hz; (b) inverse calculation of the deformation using a filter covering one pair of components around k_s ; (c) using three pairs of components; (d) using five pairs of components.

structural deformation using filtered k -spectra and equation (4), where m and n are set to zero. Figure 5(a) shows the measured deformation of the measurement area of the free-free steel plate of Figure 2(a) at 1058 Hz. Figures 5(b, c) illustrate the reconstruction of the deformation using spectral filters of various widths, including, respectively, one, three and five pairs of k -components around k_s . It can be observed that, as the spectral filter becomes wider, the reconstructed deformation approaches the measured one (but with less noise). This observation is qualitatively in accordance with the modal superposition principle and it has been used to assess the performance of the spatial Fourier transform along with the spectral filtering procedure.

6.1. REACTIVITY INTENSITY

While investigating reactive intensity, spectral filters did not appear to require a large number of k -components. In all our cases, it was noticed that, when the excitation frequency was close to one of the resonances of the plate, the filter did not need to cover more than one pair of k -components neighboring the structural wave number k_s . At off-resonant frequencies, a slightly wider filter was needed to cover two pairs of k -components. Larger numbers of k -components introduced the “smearing” effects pointed out earlier. However,

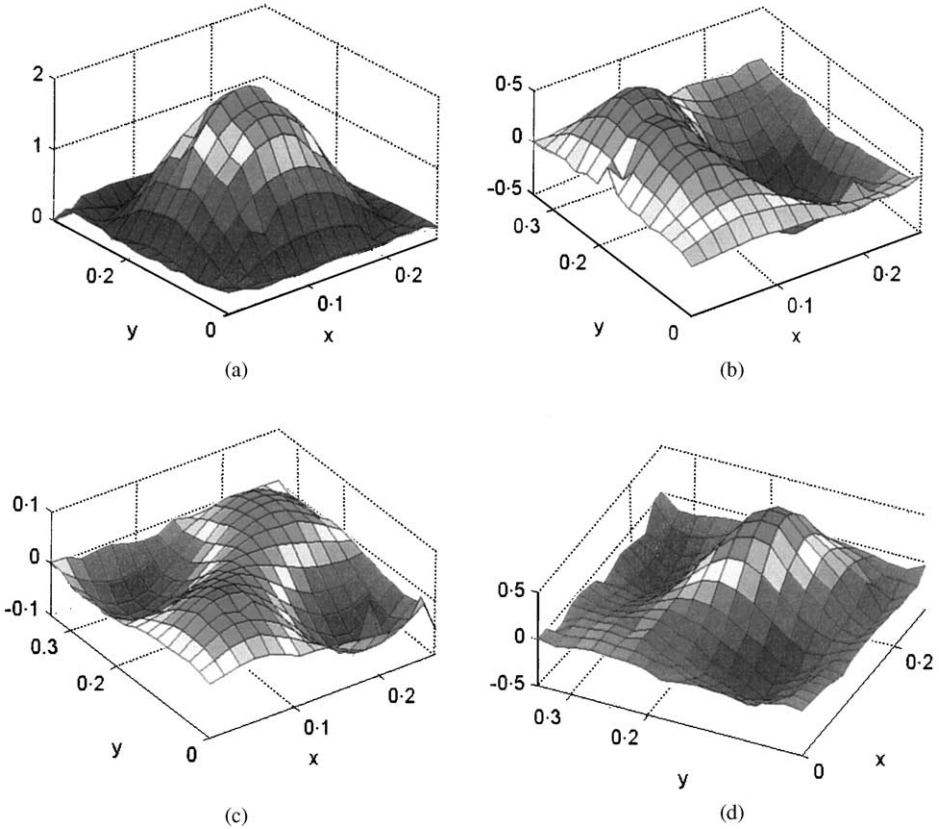


Figure 6. Flexural deformation field of the gearbox top plate: (a) 475 Hz, (b) 1092 Hz, (c) 1278 Hz, (d) 1362 Hz.

as it will be discussed later, in the context of active intensity, more components are needed to account for near field effects related to sources and discontinuities.

First, we study the top plate of gearbox of Figure 4. This plate is almost rigidly fixed at its outer boundaries resulting in very small displacements at the edges. This fact, combined with a gradual decrease in the plate stiffness with distance from the edges, produces a spatial ‘cosine’ window. It leads to a significant reduction in spectral leakage in Fourier transforms and consequently, to much more defined and recognizable structural deformations. Three examples of intensity measurements, corresponding to four different excitation frequencies, are discussed next.

First, consider an example at 475 Hz, which is very close to the eigenfrequency of the (1, 1) mode of vibration as shown in Figure 6(a). Total reactive flexural intensity and its components are shown in Figure 7. Some of these reactive parts clearly show the deformation patterns. The bending moment (Figure 7(b)) contribution reveals the convergence of the energies at the extrema of the plate deformation, suggesting a relative maximum of the reactive bending moment energy at vibration antinodes. In the shear force contribution (Figure 7(c)), the convergence of the energy takes place at the inflection points, i.e., at the nodal lines. The twisting moment contribution of Figure 7(d) shows convergence of energy toward the plate corners, where the other components are at their minimum. However, quantitatively speaking, twisting moment contributions are too small (Table 1) to leave a noticeable footprint on the total intensity field (note: sub-intensity figures do not have the same scale). The total reactive intensity in this particular case is subject to

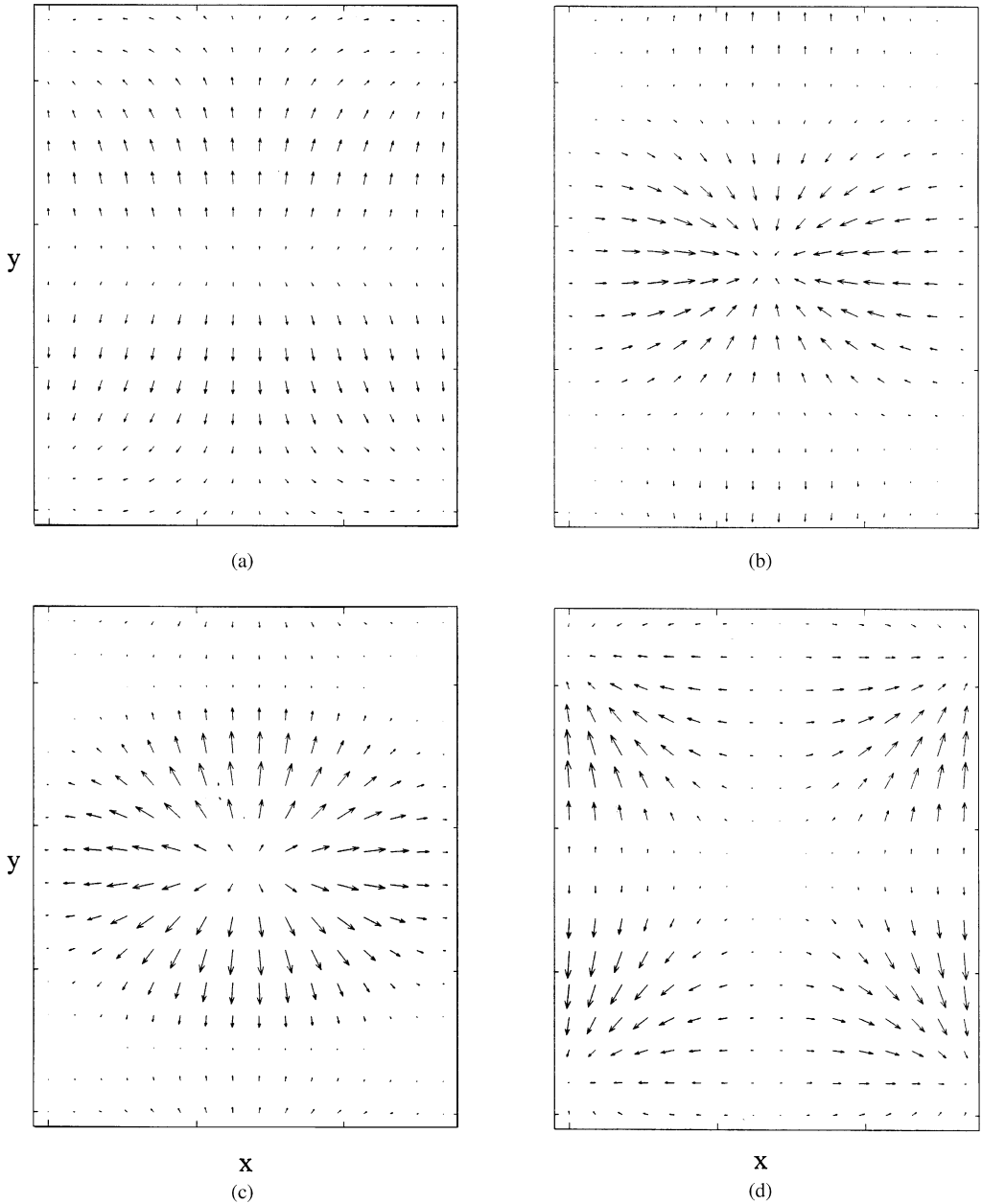


Figure 7. Flexural reactive intensity field on the gearbox plate at 475 Hz. (a) Total intensity; (b) bending moment contribution; (c) shear force contribution; (d) twisting moment contribution.

significant vector cancellations between the bending moment and shear force contributions but ultimately the shear force contribution appears dominant.

Having the above well-defined intensity patterns in mind, a concrete example of the effects of spectral filtering can now be observed. Figure 8(a) represents the bending moment sub-intensity of the above example, with no spectra filter applied. No particular pattern is detected in the field, suggesting strong cancellation effects (smearing) among the vectors due to the action of the noise within the entire wave number range.

TABLE 1

Energy contribution (intensity vector amplitude integrated over the measurement surface) from individual components of reactive intensity

Structure	Method	Frequency (Hz)	Bending moment (%)	Shear force (%)	Twisting moment (%)
A	Experimental	475 (n.r.)	41	45.5	13.5
A	Experimental	1092 (n.r.)	40	49	11
A	Experimental	1278 (n.r.)	28	59.5	12.5
A	Experimental	1362 (o.r.)	30	57	12
B	Experimental	540 (n.r.)	56	37	7

Note: A: gearbox top plate; B: free-free plate; n.r.: near resonance; o.r.: off-resonance.

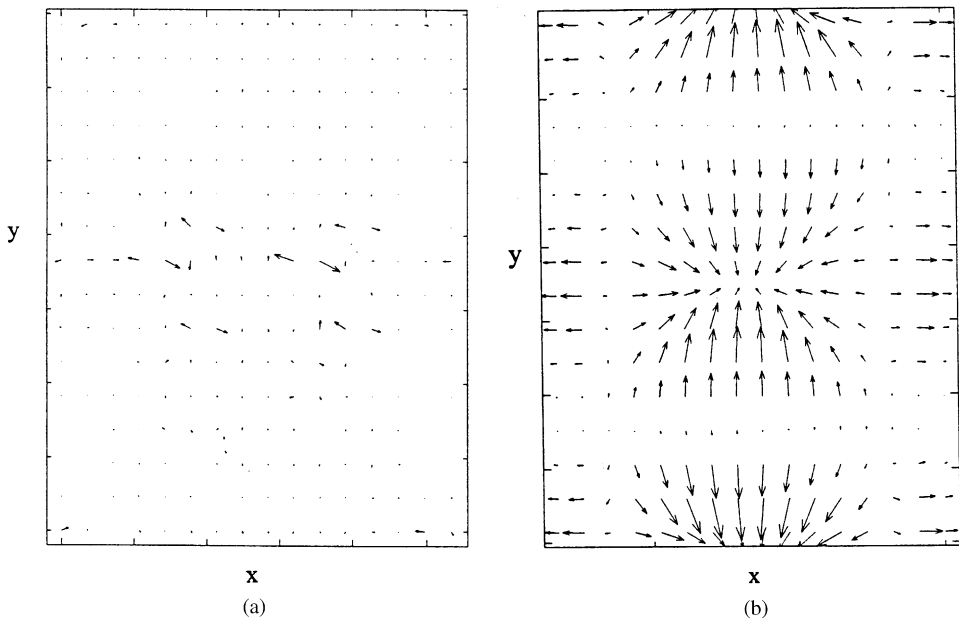


Figure 8. Reactive bending moment sub-intensity field on the gearbox top plate at 475 Hz: (a) no k -filter used; (b) using a low-pass k -filter with $f_c = 1.5 k_c$.

The measured reactive intensity behavior is consistent in all cases studied by the authors (at 11 different excitation frequencies). Hence, for the sake of brevity, the following examples will discuss only the bending moment and shear force sub-intensities.

Figures 6(b–d) represent the plate deformations at the excitation frequencies 1092 Hz (near the modes 2, 1), 1278 Hz (near the mode 2, 2) and 1362 Hz (located between two consecutive modes). Pairs of bending moment—shear force reactive sub-intensities are illustrated in Figure 9(a, b) for 1092 Hz, Figure 10(a, b) for 1278 Hz, and Figure 11(a, b) for 1362 Hz. They all show consistent trends and reflect the deformation in the same manner as described in the previous example, i.e., vector convergence at anti-nodes for bending moments and at nodal lines for shear forces.

Next, we analyze the case of a free-free plate, where only one excitation frequency of 540 Hz will be discussed. In Figure 12, the corresponding plate deformation can be seen. It

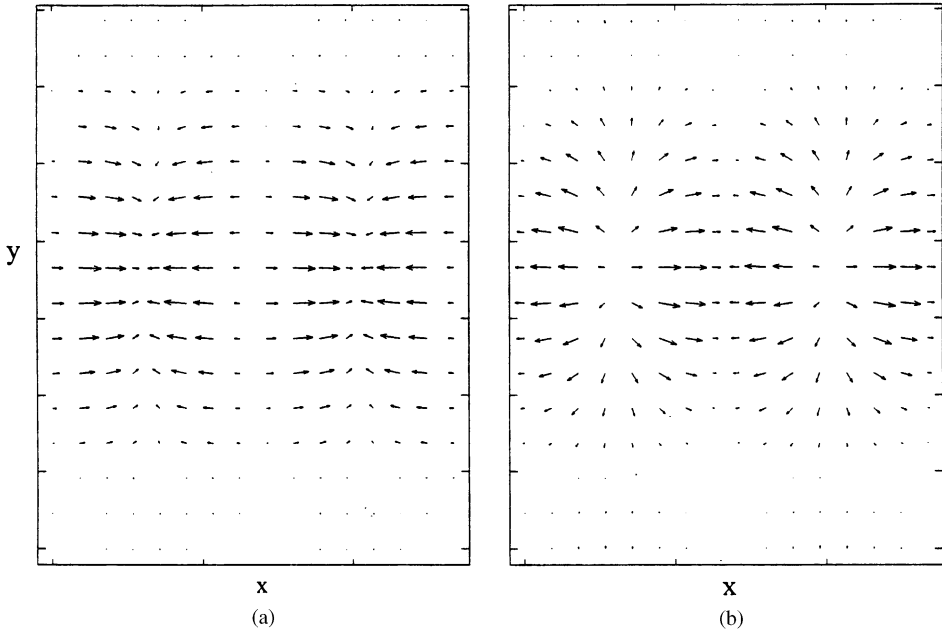


Figure 9. Reactive intensity field on the gearbox plate at 1092 Hz. (a) Bending moment sub-intensity; (b) shear force sub-intensity.

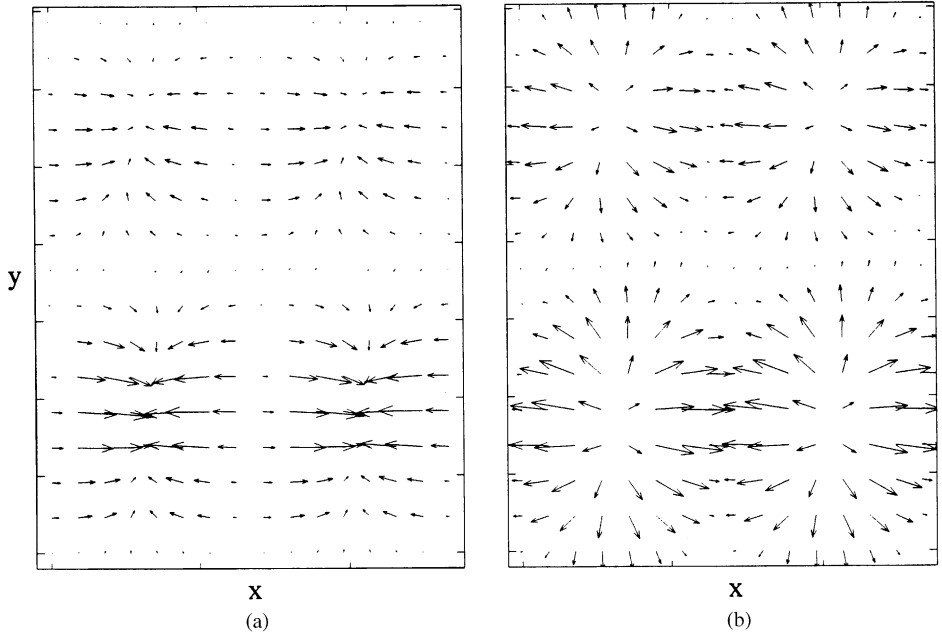


Figure 10. Reactive intensity field on the gearbox plate at 1278 Hz. (a) Bending moment sub-intensity; (b) shear force sub-intensity.

roughly demonstrates one wavelength in the x direction and no periodicity in the y direction ($2, 0$ axial mode). Note that no curve fitting or smoothing procedure has been used in this representation. Figure 13 shows the reactive shear force contribution. This

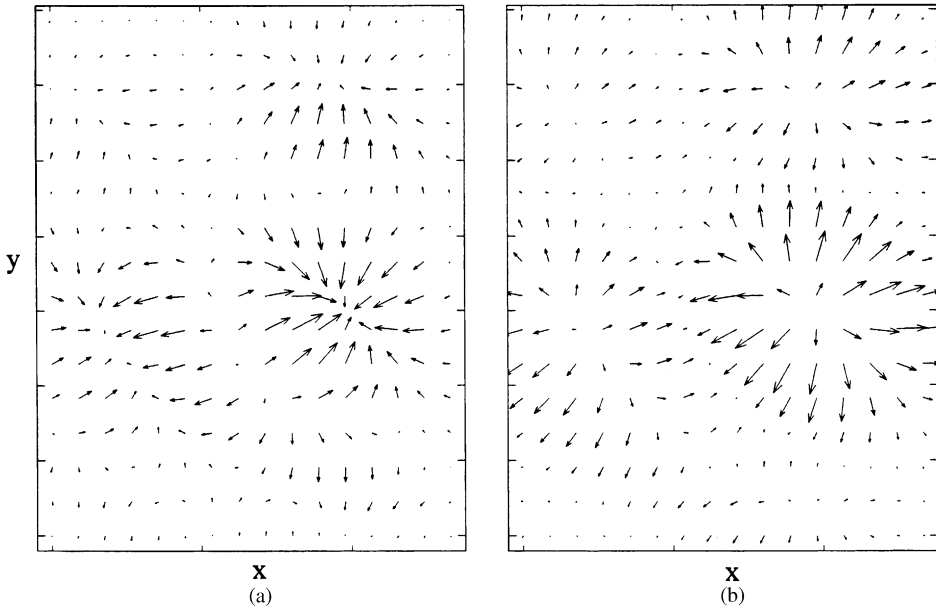


Figure 11. Reactive intensity field on the gearbox plate at 1362 Hz. (a) Bending moment sub-intensity; (b) shear force sub-intensity.

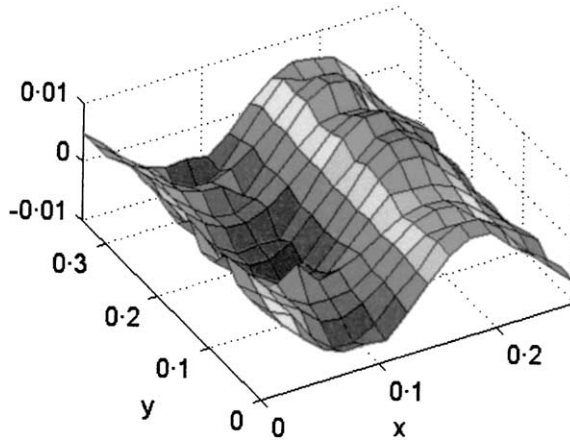


Figure 12. Forced flexural deformation field of an undamped free-free plate at 540 Hz.

pattern in which the intensity vectors diverge at the extrema corresponds well to the plate deformation.

The outcome of the examples above, i.e., reactive intensity representing the plate deformations, suggests that the classical method of vibration transmission study, based on vibration amplitude measurements, can only represent the reactive (non-propagating) part of the energy and not the transmission.

It may now be interesting to compare the results with those obtained from the application of a low-pass k -filter, as evoked in section 4.3. All these filters are basically

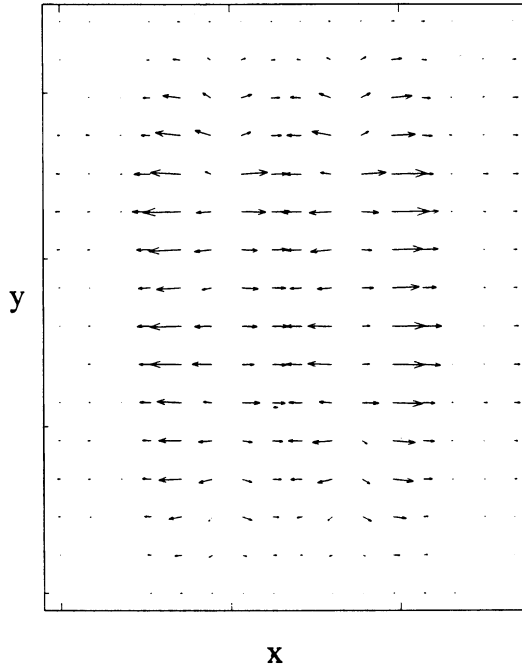


Figure 13. Reactive shear force sub-intensity field on the free-free plate at 540 Hz.

similar. The one chosen here is proposed by Williams *et al.* [3]. Figure 8(b) shows the bending reactive sub-intensity obtained at a cut-off wave number of $k_c = 1.5 k_g$. No clear indication of the natural mode (1, 1) can be observed here (as compared of Figure 7(b)). Strong intensity vectors pointing toward the upper and lower edges of the plate imply high displacement at these edges, which is obviously not the case.

6.2. ACTIVE INTENSITY

6.2.1. Excitation source near field effects

In an infinite plate, subject to flexural excitation by a point source, the following conditions hold, at the excitation point: (1) angular displacements vanish; (2) the input force emerges entirely as shear force; (3) the displacement is symmetric around the axis of excitation. These conditions, along with the decaying behavior of near fields, are expressed in terms of Hankel functions of the second kind [12]. The Fourier transforms of such functions produce exponentially decaying spectra that modulate the amplitude of the plate modal components. In this investigation of active intensity, the free-free plate's dimensions were 3–4 times greater than the flexural wavelength of the lowest excitation frequencies. Hence, the plate practically satisfies the conditions 1–3, associated with infinite plates. Moreover, although in practical situations ideal point sources do not exist, here, the very small area of excitation, compared to the applied wavelengths, justifies the point source assumption. A further important point, discussed in detail in the above reference, is the fact that the power supplied to a plate by a point source is a real or active quantity (as is the input impedance of a plate). This explains why the point sources can be localized in active, and not reactive, intensity fields.

6.2.2. Free-free plate with damping treatment in one corner

In discussing free-free plates, special emphasis will be put on source-receiver localization as one of the important tasks required from intensity investigations. In some cases, such as in undamped plates with small dimensions, this task is quite tedious if not impossible. The following experimental examples show that special treatments such as anechoic endings are not always necessary for source/sink localization. These kinds of treatment, on the other hand, may not be feasible or even judicious in practical situations.

Figure 14 represents the flexural intensity fields calculated using measured data at 1058 Hz. In Figure 14(a), the k -filter covers two pairs of k -components surrounding the structural wave number corresponding to 1058 Hz. The flow of energy toward the damping material is quite obvious. However, there is almost no evidence of the existence of the source. By widening the k -filter width to include four pairs of k -components, the intensity field now clearly displays the position of the source (Figure 14(b)). Notice that a small quantity of the source energy propagates away from the damping patches. The plate's internal damping dissipates some of this energy and the rest is reflected back from the plate untreated boundaries. These reflections however, are too weak to obscure the source location.

The fact that the source localization requires a higher number of k -components to be included in the inverse Fourier transformation, is related to the field configuration. In the region close to a source, i.e., at its near field, strong near field effects exist. Such exponentially decaying field contributes components to the whole k -spectrum, also in a decaying fashion. Defining a source position requires a higher amount of information than is necessary for the far field energy flow descriptions. This information can be provided only by a wider k -filter, corresponding to a higher number of k -components or modes. In practice however, too wide a filter may introduce more noise leading to an excessive

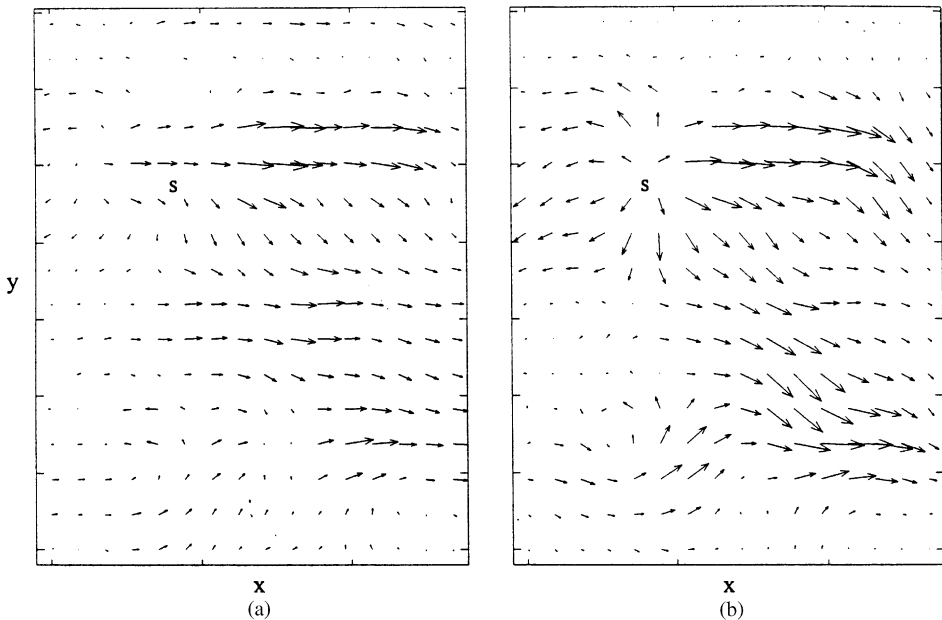


Figure 14. Flexural active intensity field on the free-free plate with damping layers in a corner, at 1058 Hz. (a) Calculated, with k -filter covering two pairs of k -components; (b) covering four pairs of k -components.

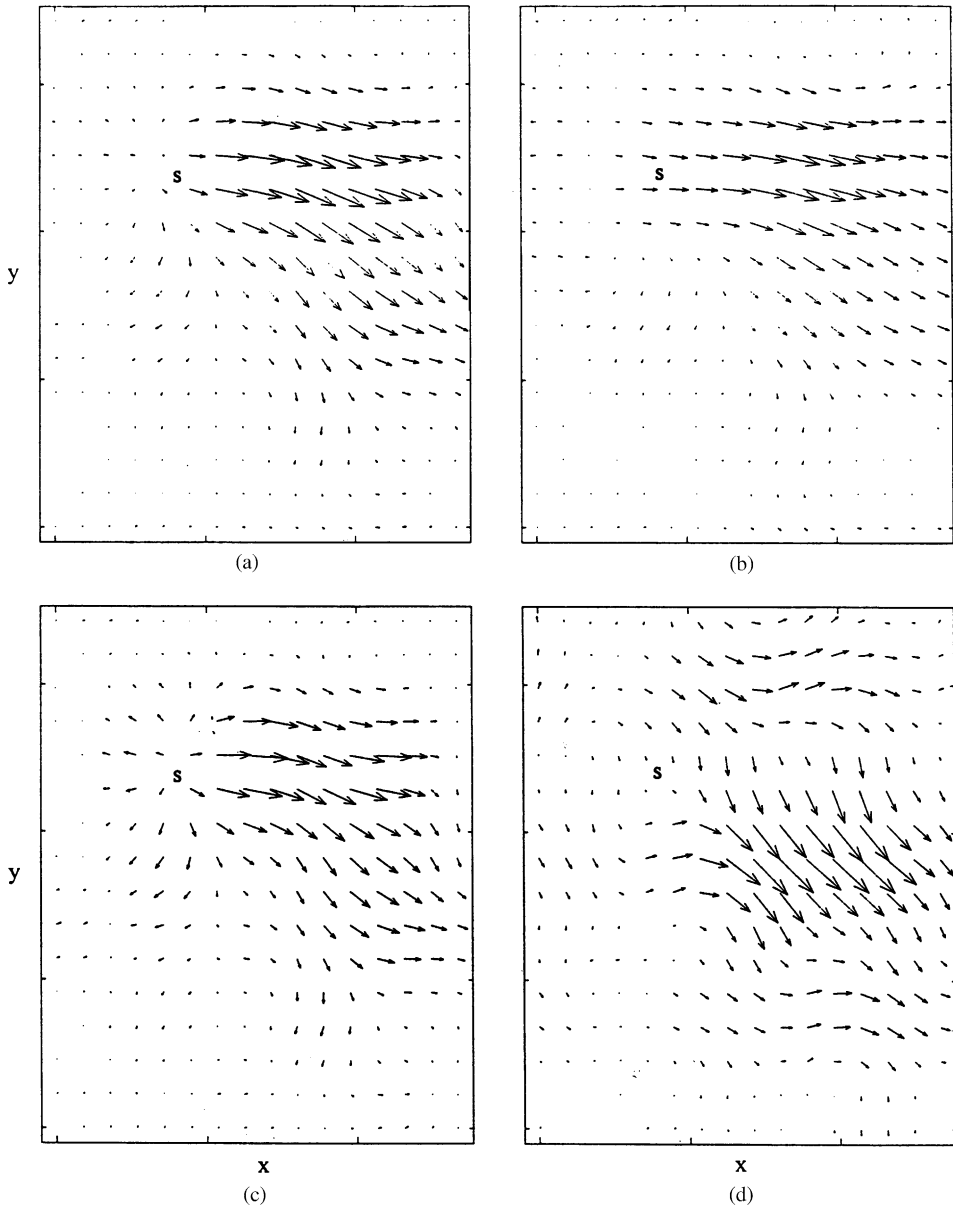


Figure 15. Free-free plate with damping layers in a corner, at 496 Hz. (a) Flexural active intensity; (b) bending moment contribution; (c) shear force contribution; (d) twisting moment contribution.

smearing of the field, as described earlier. Estimation of intensity, therefore, demands a compromise in choosing the k -filter width.

Figure 15 presents another example of the intensity in the plate at 496 Hz, where k_s is located between modes (0, 3) and (2, 2). In this figure the total flexural intensity (Figure 15(a)) has been shown along with its three components, i.e., bending moment, shear force and twisting moment contributions (Figure 15(b-d); again note in these sub-figures, the scales are not the same). As seen earlier, the twisting moment contribution appears to be quite insignificant, compared to those of shear forces and bending moments (Table 2).

TABLE 2

Energy contribution (intensity vector amplitude integrated over the measurement surface) from individual components of active intensity

Structure	Method	Frequency (Hz)	Bending moment (%)	Shear force (%)	Twisting moment (%)
A	Experimental	496 (o.r.)	36	52	12
A	Experimental	1058 (o.r.)	35	52	13
B	Experimental	821 (o.r.)	34	53	13
B	Experimental	1047 (n.r.)	40.5	50	9.5
B	Experimental	1058 (n.r.)	34	54	12
B	Experimental	1149 (n.r.)	33	54	13
C	Experimental	543 (n.r.)	35	55	10
C	Experimental	821 (o.r.)	38	50	12
D	Experimental	553 (n.r.)	41	49	10
D	Experimental	1443 (o.r.)	36	50	14
E	Experimental	1092 (n.r.)	40	46	14
E	Experimental	1362 (o.r.)	32	54	14
F	FEM	483 (o.r.)	34	52.5	13.5
F	FEM	836 (res)	41	47	12

Note: A: Free-free plate, damping in a corner; B: same without damping; C: same, damping all around the edges; D: irregularly shaped free-free plate; E: gearbox plate; F: analytical FE model with $\zeta = 0.5\%$; n.r.: near resonance; o.r. off-resonance; res: resonance.

Accordingly, Figure 15 shows the relative insensitivity of the total intensity with regard to the twisting moment contribution, and the dominance of the other two. The shear force on the other hand, is the main component leading to the source localization, as it can be seen in Figure 15(c). The reason is that at the source position, bending and twisting moments are negligible while the shear forces are quite strong.

6.2.3. Free-free steel plate with no damping treatment

The same structure as in section 6.2.2, but with constrained damping layers removed, was used in which only the plate's internal (and small) damping as well as some sound radiation constitute the main mechanism of energy dissipation in the system. Because of the lack of a concentrated energy sink or any localized absorption in such a system, it is not expected that any regular and well-defined stream of energy be observed. This is because the energy flow pattern is conditioned by the edge reflections and by the non-homogeneity of the material property and internal damping. However, the possibility of source localization still exists. In Figure 16, the shear force sub-intensities at 821 and 1149 Hz, display the source location in an acceptable manner. In Figure 17(a) however, the shear force sub-intensity corresponding to 1058 Hz, hardly reveals the source position, while in Figure 17(b) (1047 Hz) no source is detected at all.

It can be argued that when high-energy modes are being excited (which is the case of 1058 and 1047 Hz, where the structure is being excited at or near its resonance frequencies) then strong boundary reflections are formed in the intensity field. These phenomena can obstruct the source position. In contrast, the lower energy modes appear, when the excitation takes place at off-resonance frequencies (e.g., at 1058 and 1047 Hz). The reflected energies from the plate edges are, in this case, weak and may be completely dissipated in their path.

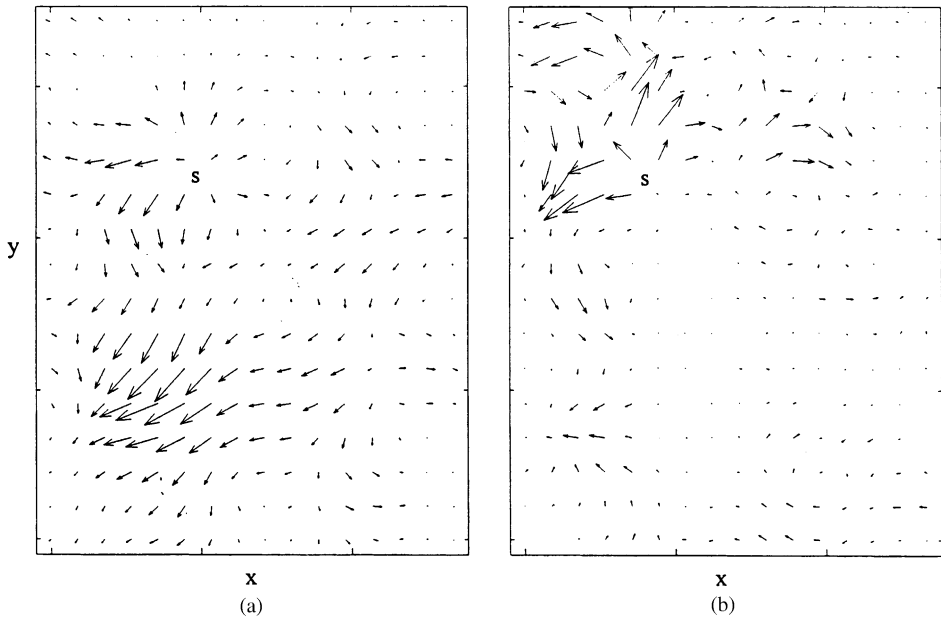


Figure 16. Active shear force sub-intensity field on the free-free undamped plate: (a) at 821 Hz, (b) at 1149 Hz.

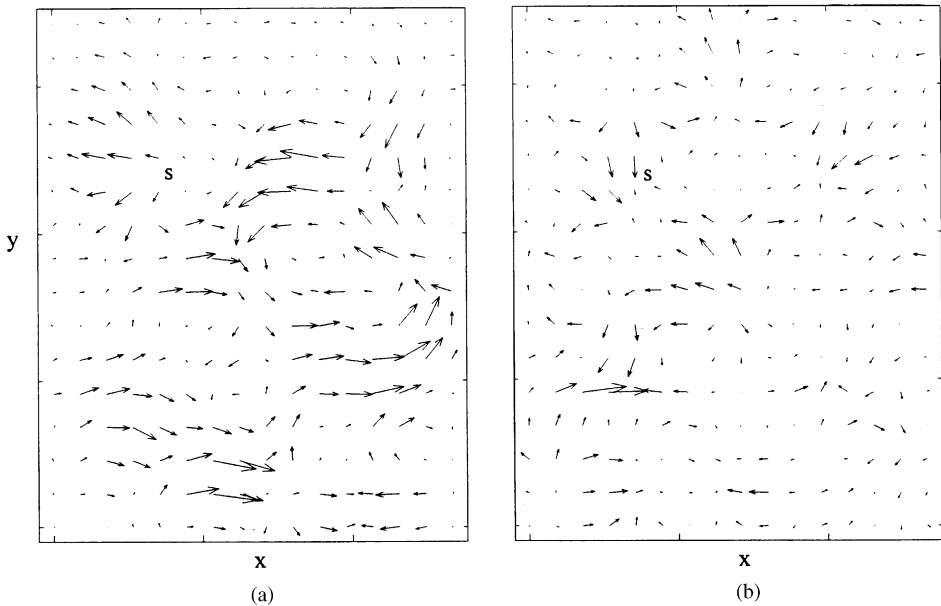


Figure 17. Active shear force sub-intensity field on the free-free undamped plate: (a) at 1058 Hz, (b) at 1047 Hz.

6.2.4. Plate with constraint layer damping along all the edges

When the damping is provided all around the edges, the corresponding reflections are considerably weakened and therefore their impact on source localization, as observed in the previous structure, is reduced. The sources are now easily detected even at resonance

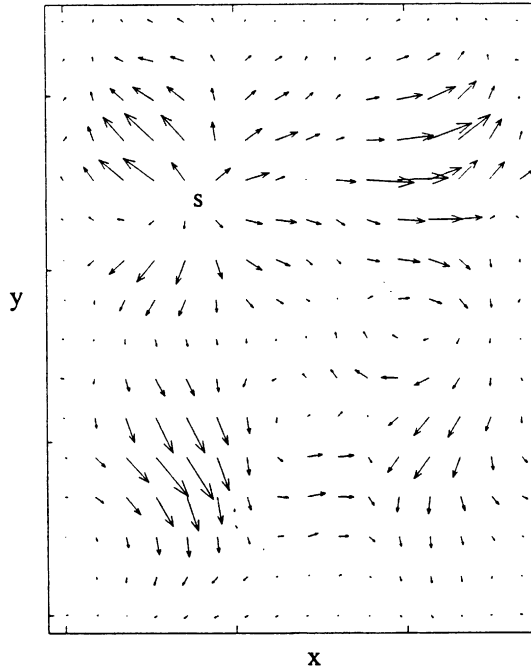


Figure 18. Active shear force sub-intensity field on the free-free plate with damping along all the edges at 543 Hz (near-resonance).

frequencies as shown in Figure 18 corresponding to the shear force sub-intensity at a near resonance frequency of 543 Hz. This observation proves the argument presented in the previous paragraph, with regard to the difficulty involved in source localization at resonance frequencies. The energy streams flow toward the edges. The pattern and direction adopted by these streams are dictated by the non-uniformity of the damping patches and the plate material.

6.2.5. Irregularly shaped free-free plate

The irregularly shaped plate of Figure 2(d) was processed in the same way as the regular plates. It was found that a rectangular measurement zone could still be used on such an irregular plate. This technique allows to visualize the flow of energy and to localize the source, as can be seen in Figure 19, where the active shear force sub-intensity corresponding to the excitation frequency of 553 Hz is illustrated. This is an important result because it suggests that the technique is adaptable for complex plate geometries, which is the case in most realistic structures.

6.2.6. Active intensity on a gearbox plate

Two examples of active intensity will be discussed for this case. First, consider the excitation at 1092 Hz. At this frequency the plate deformation is dominated by the mode (2, 1) of the plate. Figure 20 represents the total active flexural intensity (Figure 20(a)) along its components, i.e., bending moment, shear force and twisting moment contributions (Figure 20(b-d)). The main (in terms of quantity, see Table 2) components, i.e., the shear force and bending moment sub-intensities, and consequently, the total intensity itself, clearly demonstrate a stream of energy coming from the right lateral plate of the box. This

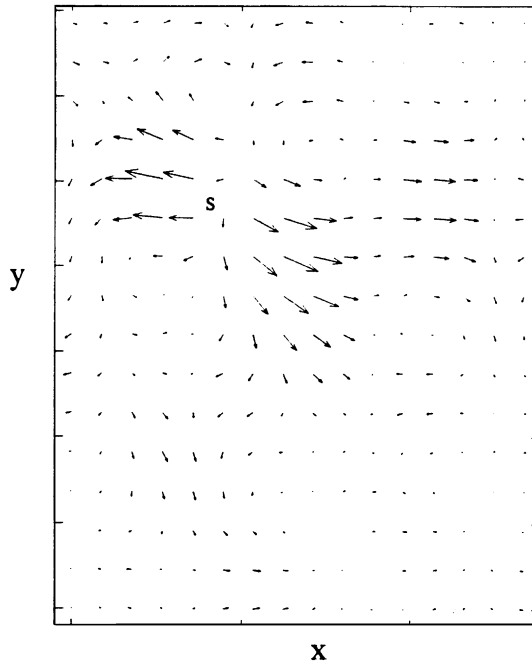


Figure 19. Active shear force sub-intensity field on the free-free irregular plate at 553 Hz.

energy flows across the top plate and runs into the box's left lateral plate. Another example corresponds to the excitation frequency of 1362 Hz. In Figure 21, each sub-figure represents the total intensity at a different spectral filter width (the effect of the width is discussed in the context of smearing, in the following sub-section). The intensity field looks more involved than the preceding example. Here, all four lateral plates of the box seem to be active in providing or receiving energy to or from the upper plate. The abnormally short intensity vectors at the edges of the plate are the direct consequence of measurement noise. The plate edges have been fixed to the rest of the box, using a number of screws. Hence, the amplitudes of vibration at the edges are very small and lead to low measurement signal-to-noise ratios.

From the above examples, a conclusion may be drawn that is of important practical consequence: although the displacement amplitudes along the plate's edges are quite small, the overall intensity pattern shows a significant amount of energy crossing them. This further confirms the conclusion drawn from the analysis of the reactive intensity (section 6.1), i.e., in studying the transmission across discontinuities, high (normal) vibration amplitudes do not necessarily imply a high energy transmission.

6.2.7. Smearing effects

In many intensity field representations, unexpected variation in the amplitude of the intensity vectors may be observed in locations where neither energy sources nor sinks are present. Such results may be interpreted as illogical and inaccurate, however, an important reason may lie behind such phenomena referred to, in previous sub-sections, as "smearing" effect. Although plate-edge reflections and non-uniformity of the material property and damping distribution can cause such effects, they are mainly the consequence of the accumulation of the uncorrelated noise within the k -filters. Larger spectral k -filters incorporate more noise leading to more "smearing" in the intensity field. In Figure 21, four

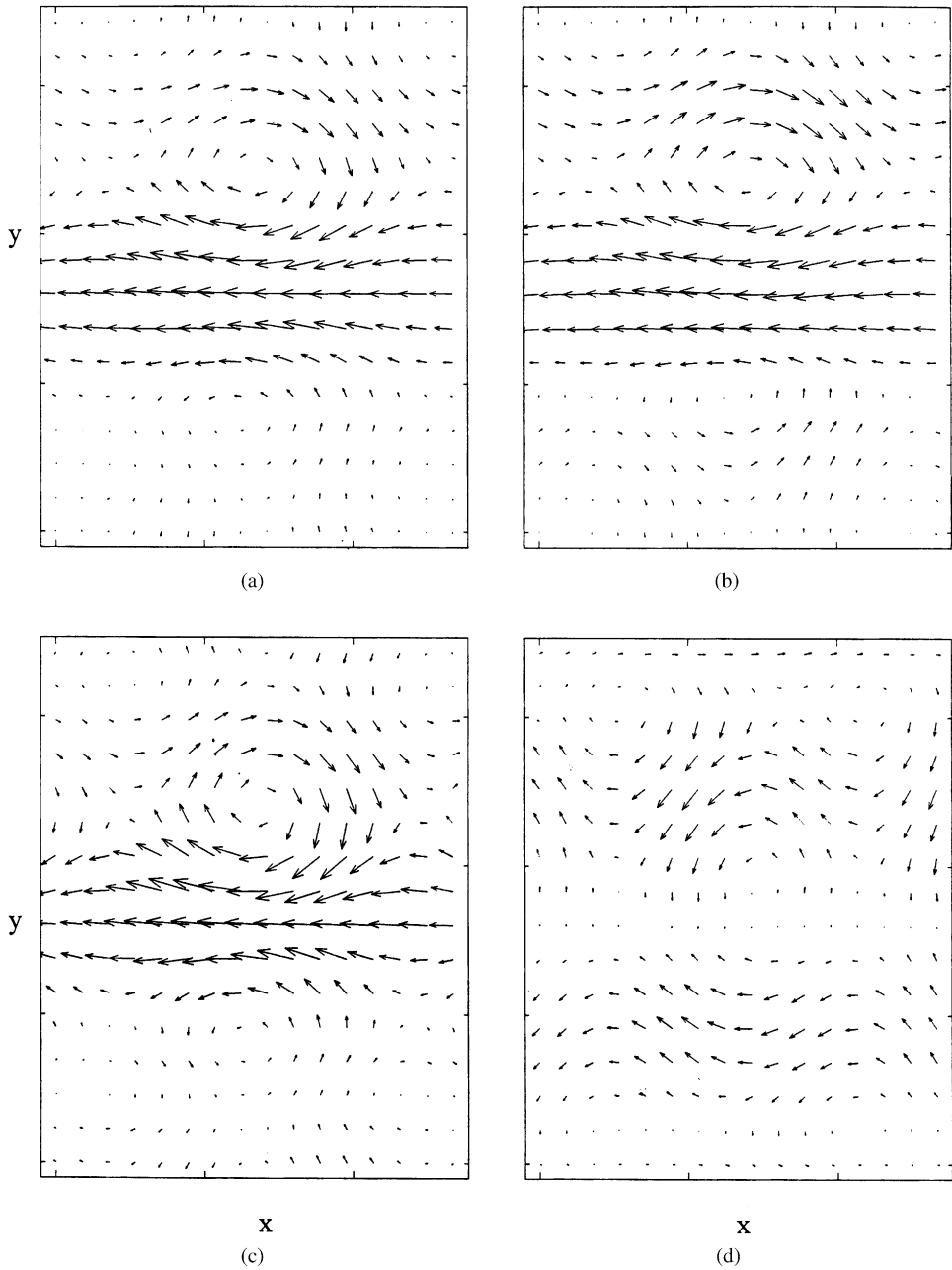


Figure 20. Top plate of the gearbox at 1092 Hz. (a) Total active intensity; (b) bending moment sub-intensity; (c) shear force sub-intensity; (d) twisting moment sub-intensity.

“variants” of the total intensity on the gearbox plate demonstrate the effects of widening the k -spectral filter. Figures 21(a–d) are related to the filters that include 1, 2, 6 and 10 pairs of k -components around k_s , respectively. It can be observed how wider filters can lead to fields with irregularly localized changes in the norms of the intensity vectors. The analytical studies (section 7) further confirms noise as the main agent of the “smearing”.

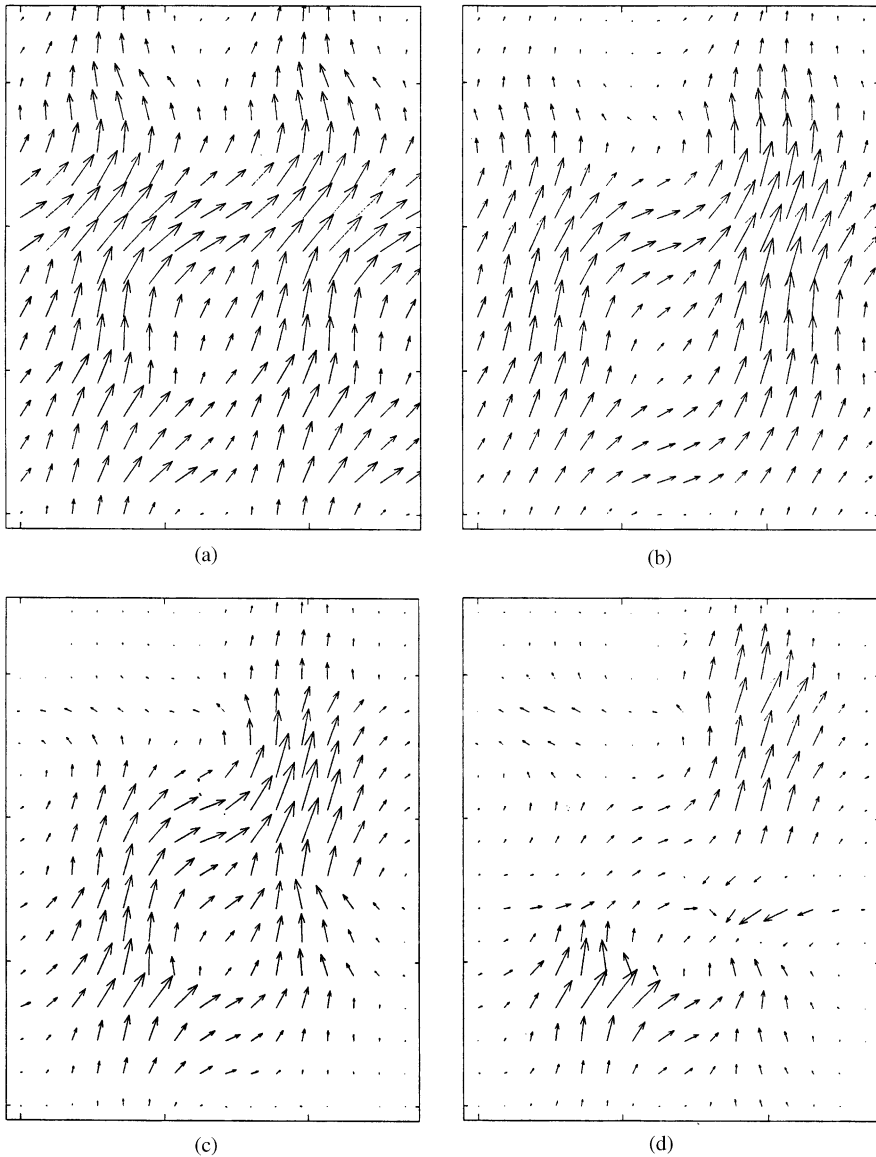


Figure 21. Smearing effect in the intensity calculations. Gearbox plate at 1362 Hz. (a) k -filter covering one pair of k -components adjacent to k_s ; (b) with two pairs of k -components; (c) with six pairs; (d) with 10 pairs.

6.2.8. Acoustic radiation and flexural intensity

Theoretically speaking, the sound radiated from finite rectangular free-free plates in the subsonic region is insignificant. For this reason, the investigation on structure borne sound was implemented on the top plate of a rotorcraft gearbox with fixed boundaries. The aim is to explore the possibility of establishing a link between the flexural intensity and the intensity of the associated sound radiation.

An extensive analysis, covering both subsonic (where $\lambda_b < \lambda_{sound}$) and supersonic (where $\lambda_b > \lambda_{sound}$) frequency zones, has been carried out. The acoustic and flexural intensity fields were studied in parallel. These studies show that the evidence of sound radiation can be

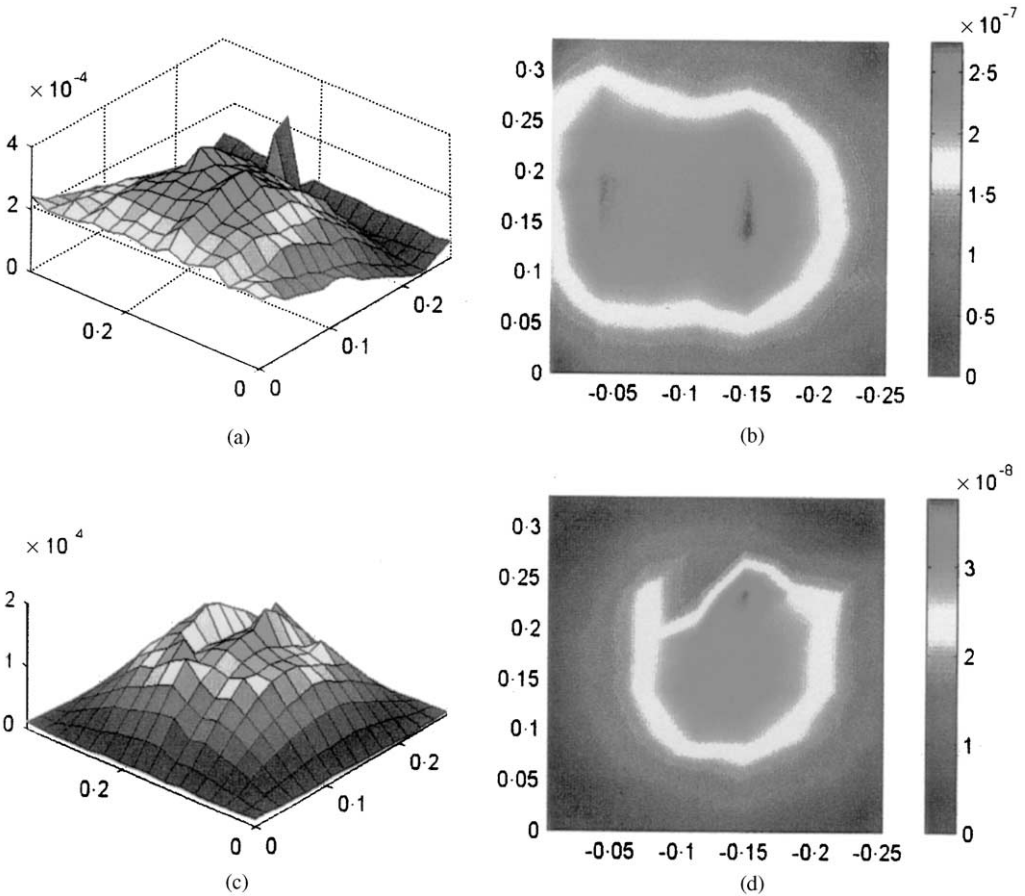


Figure 22. Gearbox top plate: (a) deformation at 357 Hz; (b) radiated sound intensity at 357 Hz; (c) deformation at 421 Hz; (d) radiated sound intensity at 421 Hz.

observed on flexural intensity fields only in cases where a significant portion of the surface radiates. At subsonic regions this is true only when the motion of the whole plate is in phase, e.g., at frequencies corresponding to 1, 1 modes. At the other frequencies, strong acoustic cancelling effects [4] take place that dramatically reduce the radiating surface areas. These effects are further reinforced by the presence of the multitude of eigenmodes excited by one single excitation frequency. Two examples are presented here. Figure 22 illustrates the plate deformations and the sound intensity at the frequencies 357 and 421 Hz, where the plate goes through an in-phase motion. It can be seen that the radiation is emitted from a large portion of the surface. Figure 23 represents the associated total flexural (a and c) and shear force (b and d) active sub-intensities. The energy convergence to the middle of the plate, where no energy sink is present, suggests the release of the energy into the air in forms of radiation. This effect is more obvious in the shear force component of the intensity suggesting also that the acoustic radiation be affiliated to shear forces rather than to the moments.

At supersonic regions, although the overall radiation is higher than in subsonic zones, the radiation surfaces are comprised of small patches as illustrated in two examples of Figure 24. Here, no evidence of such radiation could be detected in the flexural intensity field.

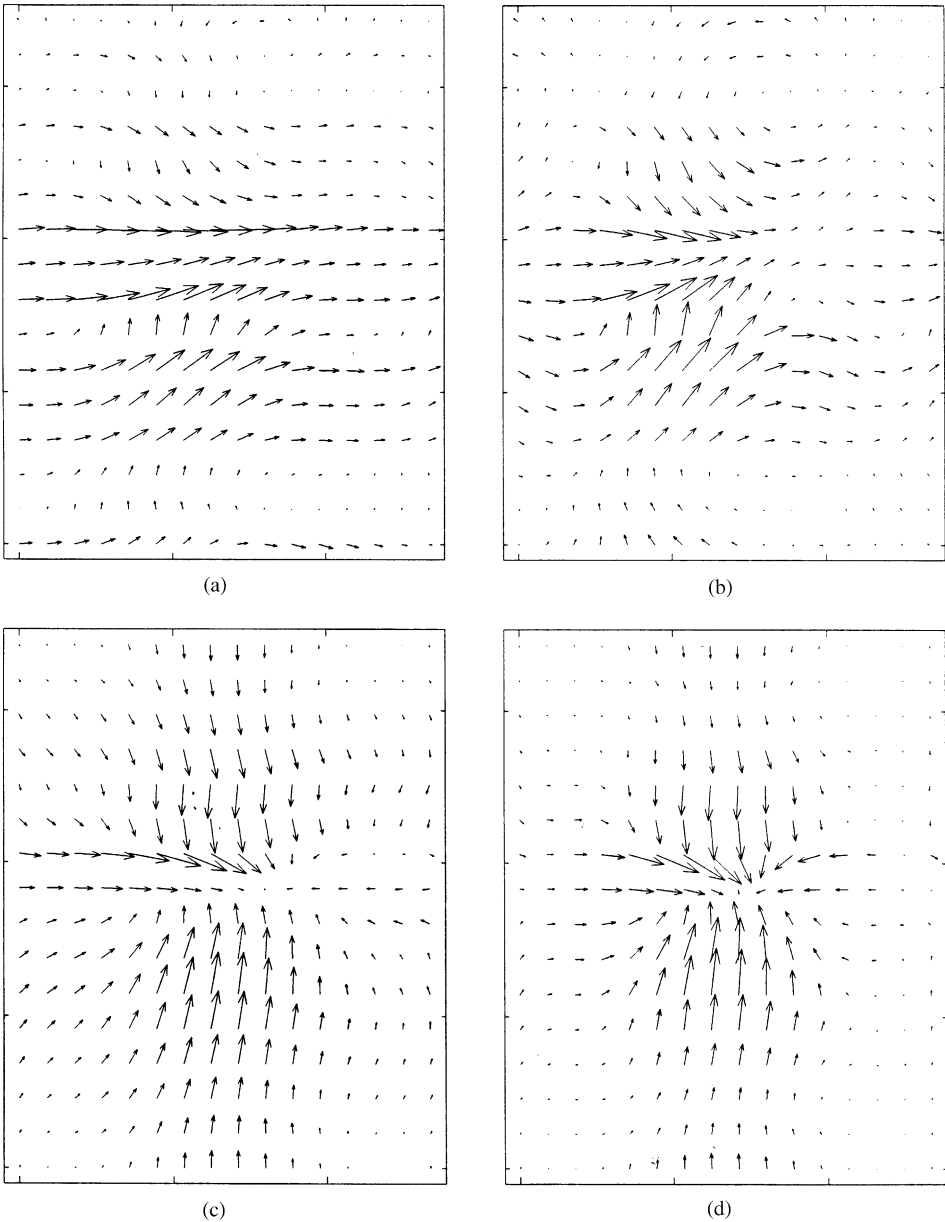


Figure 23. Structural intensity field on the gearbox top plate. (a) Total flexural intensity at 357 Hz; (b) shear force sub-intensity at 357 Hz; (c) total flexural intensity at 421 Hz; (d) shear force sub-intensity at 421 Hz.

7. FINITE ELEMENT ANALYSIS

In section 6.2.7, it was suggested that the 'smearing' phenomenon would be caused by uncorrelated noise and plate edge reflections. It is interesting therefore, to examine the validity of such arguments in an ideal system, i.e., free of noise and where the edge reflections could be controlled. To do so, a computational investigation is carried out using the finite element method. A steel plate of dimensions $900 \times 900 \times 2.5 \text{ mm}^3$, $E = 2e^{11} \text{ Pa}$, $\nu = 0.3$ and

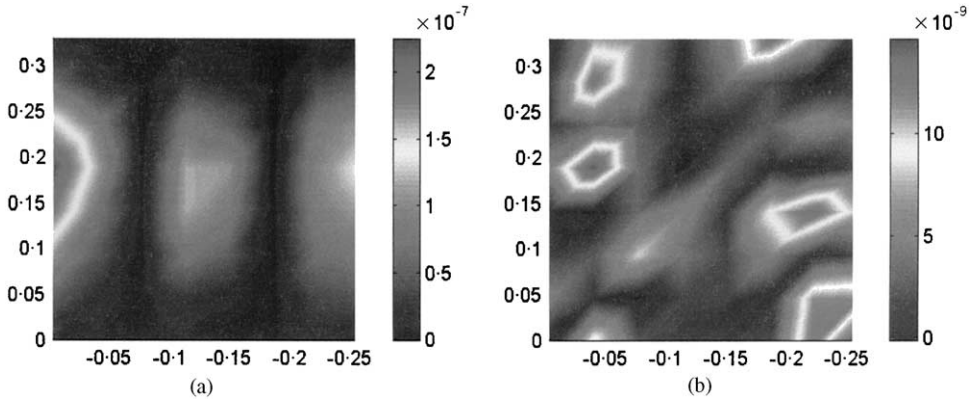


Figure 24. Examples of radiated sound intensity, at supersonic region, from the gearbox top plate: (a) at 2220 Hz, (b) 2995 Hz.

$\rho = 7800 \text{ kg/m}^3$ is modelled using the ANSYS software [17]. A harmonic force of unit amplitude is applied on the plate at the coordinates (391, 378 mm). The model incorporates a 50×40 grid providing 2000 four-node shell elements. Natural frequencies are obtained through the block Lanczos solution [17] and the force response functions are calculated using the modal superposition approach. Calculation of structural intensities was subsequently carried out using the above complex transfer functions (cross-mobilities), along with the formulas and techniques described in sections 2 and 3. These calculations were implemented on a smaller ($576 \times 720 \text{ mm}^2$) area in the middle of the plate that covers 32×32 nodes and includes the excitation point. Results from various types of ideal boundary conditions were found to be consistent. Therefore only the clamped-clamped boundary condition will be presented here, at two excitation frequencies of 483 Hz (off-resonance) and 836 Hz (resonance) and only the active intensity will be discussed.

It was hypothesized, in the previous sections, that smearing is caused mainly by uncorrelated noise. If true, then in an ideal noise-free system, such as the present FE model, widening of the k -filter must not lead to smearing. It was indeed observed that filters wider than 4 (6, 10, 12, 16) pairs of k -components produced no noticeable change in the pattern of the field.

Figure 25 shows the shear force intensity at 483 Hz. Here, the location of excitation source is clearly displayed. The behavior of the intensity field is, however, erratic and random energy streams are observed. This behavior, caused by interactions among outgoing source energy and the plate edge reflections, is in agreement with those observed in the experimental results and discussed in sections 6.2.3 and 6.2.4. Also, notice that, by increasing the amount of structural damping to the system (Figures 25(a-c) corresponding to the damping ratios ζ of 0.5%, 5% and highly idealized 50%, respectively) a more regular and symmetric field shape is obtained. It was also argued, in those subsections, that the edge reflections being even more energetic at resonance frequencies, may completely mask the excitation source. The analytical example in Figure 26, corresponding to the resonance frequency of 836 Hz, further verifies this analysis. Figure 26(a) represents the plate with a structural damping ratio $\zeta = 0.5\%$ which is typical in steel. In this case no source can be detected. When this ratio is increased to 5%, the source starts to emerge and the field appears much less turbulent (Figure 26(b)). In the idealized case of $\zeta = 50\%$ (Figure 26(c)), the intensity field emerges completely symmetric and the damping trend quite uniform. This investigation shows the importance of some damping in source localization. Regarding the

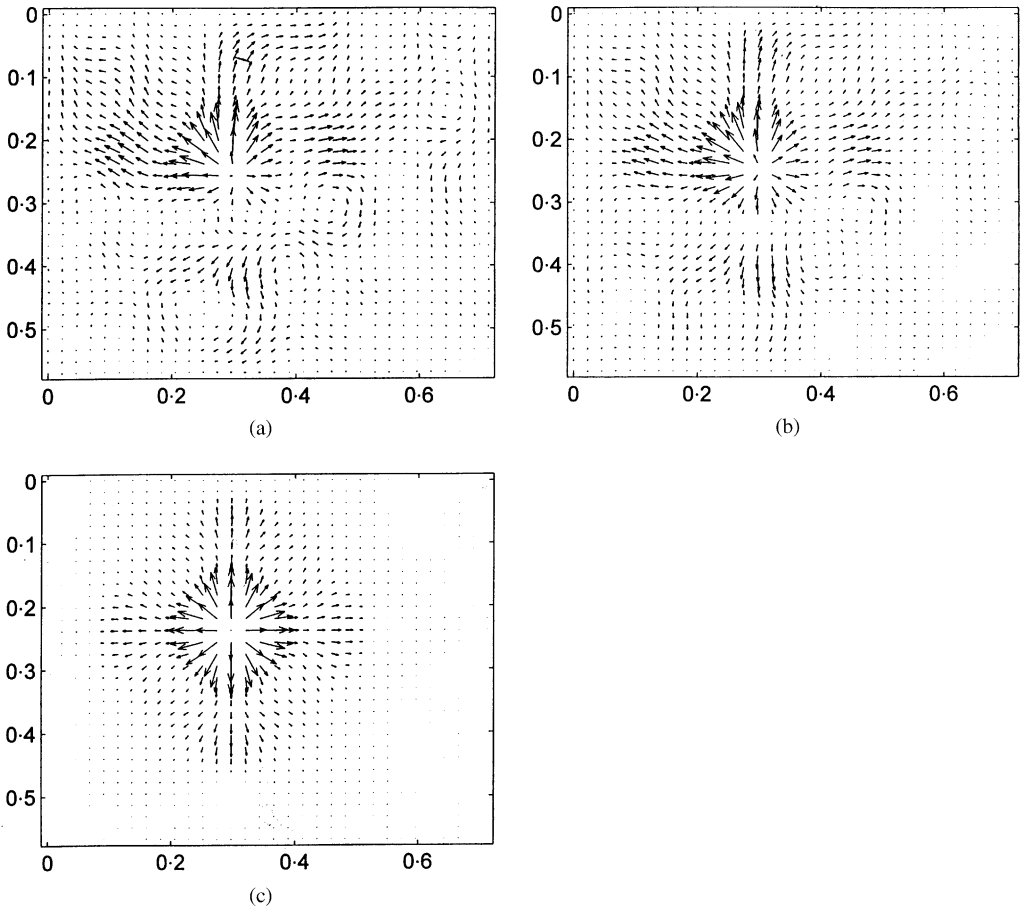


Figure 25. Shear force sub-intensity field in the middle of FE modelled plate at off-resonant frequency of 483 Hz; (a) with $\zeta = 0.5\%$; (b) with $\zeta = 5\%$; (c) with $\zeta = 50\%$.

quantitative comparison between the analytical and experimental investigation, one can observe a reasonable consistency; various contributions to total flexural intensity, from shear forces, bending and twisting moments, are quite similar in both cases (Table 2).

8. CONCLUSION

Use of spatial Fourier transforms in the estimation of structural intensity requires close attention to the modal behavior of structures and the principle of modal superposition. Although the vibration field of a structure is defined by all the excited modes, one cannot include all these modes in the intensity calculations because, in the measured data, the spectral k -components related to many of these modes may contain undesirable information such as uncorrelated noise.

The method presented here uses an ideal band-pass filter centered at the structural wave number k_s . The choice of the k -filter bandwidth depends on the aim of the application, e.g., whether the sources or sinks are to be studied or the transmission paths. This choice obligates a compromise between spectral information and noise.

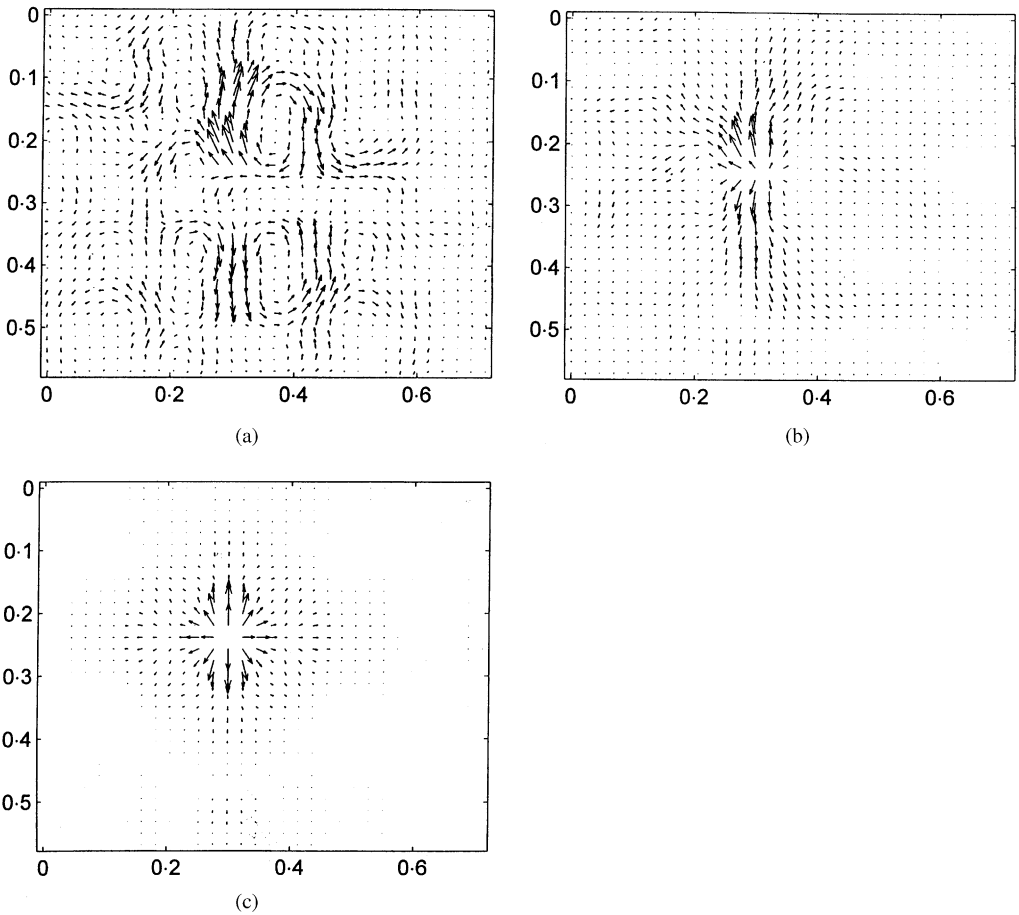


Figure 26. Shear force sub-intensity field on the middle of FE modelled plate at resonant frequency of 836 Hz: (a) with $\zeta = 0.5\%$; (b) with $\zeta = 5\%$; (c) with $\zeta = 50\%$.

Flexural intensity includes contributions from the bending moments, the shear forces and the twisting moments. The present study suggests that bending moment and shear force reactive sub-intensity fields represent the operating deformation shapes of the structure. This observation leads to the following practical conclusion. In the classical method of vibration transmission analysis, based on the measurement of vibration amplitudes, higher amplitude on a certain transmission path would imply a higher vibration transmission through that path. This is not necessarily true because, according to the present investigation, the vibration amplitudes are in fact associated with the reactive intensity, which is non-propagating. Such measurements may therefore be quite misleading in transmission path analysis and ranking. Active structural intensity is the realistic approach to such a problem.

Calculated active intensity fields clearly display source and absorption locations, as well as the energy paths even in irregularly shaped and in undamped plates with various boundary conditions. In the case of transverse excitations, such as a shaker, the shear force component is the most efficient, among the three components of flexural intensity, in identifying the source. The reason is that in this type of excitation, the moments (bending and twisting) near the source are negligible.

In undamped plates, at resonance frequency excitations, strong energy reflections from boundaries and discontinuities occur that may mask the source locations. It was observed, in FEM investigations, that the introduction of more damping in the structure could control the effects of the edge reflections. However, further work is needed to develop a different technique, rather than addition of damping, to overcome the problem of source obstruction at resonance frequencies.

Regarding the effects of sound radiation on flexural intensity, only at frequencies where the motion of the whole plate is in phase, one can see a clear transformation of vibration energy into sound energy, because a large area of the plate surface radiates. At other frequencies, radiation takes place at small areas, leaving no possibility of visualization in the flexural intensity fields.

ACKNOWLEDGMENTS

The authors would like to thank Professor G. Baker of the Mathematics Department at The Ohio State University for his advice.

REFERENCES

1. D. U. NOISEUX 1970 *Journal of Acoustical Society of America* **47**, 238–247. Measurement of power flow in uniform beams and plates.
2. G. PAVIC 1976 *Journal of Sound and Vibration* **49**, 221–230. Measurement of structure borne wave intensity. Part I: formulation of the method.
3. E. G. WILLIAMS, H. D. DARDY and R. G. FINK 1985 *Journal of Acoustical Society of America* **78**, 2061–2068. A technique for measurement of structure-borne intensity in plates.
4. F. FAHY 1985 *Sound and Structural Vibration*. New York: Academic Press.
5. Y. ZHANG and J. ADIN MANN III 1996 *Journal of Acoustical Society of America* **99**, 345–353. Measuring the structural intensity and force distribution in plates.
6. Y. ZHANG and J. ADIN MANN III 1996 *Journal of Acoustical Society of America* **99**, 354–361. Examples of using structural intensity and the force distribution to study vibrating plates.
7. A. J. ROMANO, P. B. ABRAHAM and E. G. WILLIAMS 1990 *Journal of Acoustical Society of America* **87**, 1166–1175. A poynting vector formulation for thin shells and plates, and its application to structural intensity and source localization. Part I: theory.
8. A. SPALDING and J. ADIN MANN III 1995 *Journal of Acoustical Society of America* **97**, 3617–3624. Placing small constrained layer damping patches on a plate to attain global or local velocity changes.
9. R. MORIKAWA and S. UEHA 1996 *Journal of Acoustical Society of America* **99**, 2913–2921. Error evaluation of the structural intensity measured with a scanning laser Doppler vibrometer and a k -space signal processing.
10. L. GAVRIC and G. PAVIC 1993 *Journal of Sound and Vibration* **164**, 29–43. A finite element method for computation of structural intensity by the normal mode approach.
11. O. M. BOUTHIER and R. J. BERNHARD 1995 *Journal of Sound and Vibration* **182**, 149–164. Simple models of the energetics of transversely vibrating plates.
12. L. KREMER and M. HECKL 1988 *Structure-Borne Sound* Berlin: Springer-Verlag; second edition.
13. MATLAB 1993 *User's Guide*. Natick, MA: The Math Works, Inc.
14. R. G. VOIGT, D. GOTTLIEB and M. Y. HUSSAINI 1984 *Spectral Methods for Partial Differential Equations*. PA: Philadelphia, SIAM.
15. D. J. EWINS 1986 *Modal Testing: Theory and Practice*. Letchworth, Herts: Research Studies Press Ltd.
16. W. WEAVER JR., S. P. TIMOSHENKO and D. H. YOUNG 1990 *Vibration Problems In Engineering*. New York: John Wiley & Sons; fifth edition.
17. ANSYS 1989 *User's Manual*. Swanson Canonsberg, PA: Analysis Systems, Inc.

APPENDIX A: NOMENCLATURE

D	flexural stiffness
f_r	resonant frequency
h	plate thickness
k_x, k_y	wave numbers in x and y directions respectively
$k_{m,n}$	mode (m, n) wave number
k_s	structural wave number
L	spatial record length
L_x, L_y	record lengths in x and y directions respectively
m, n	integers
N	number of samples
r	modal index
r_m, r_n	wave numbers associated with m th and n th axial modes in x and y directions respectively
S	frequency sweep rate
\tilde{W}	displacement in frequency domain
\tilde{W}	complex velocity in frequency domain
ζ	structural damping ratio
η	damping loss factor
η_r	modal loss factor
ω	cyclic frequency
ω_r	undamped natural frequency
ρ_s	plate surface density
λ_B	flexural wavelength
λ_{sound}	sound wavelength
ν	the Poisson ratio
ψ_r	eigenvector r
$[\phi]_r$	normal eigenvector r
$=$	complex quantity
$/$	complex conjugate
\top	transpose of a matrix
$\langle \rangle_t$	average in time domain